High-throughput, next-generation sequencing (NGS) has had a tremendous impact on human genetic research (22). Moreover, techniques enabling enrichment of selected regions enable us to use NGS efficiently and to identify the causative genes for a reasonable number of genetic disorders as well as susceptibility genes for complex diseases and health-related traits (23). In particular, X-linked disorders are good candidates for exome sequencing. We recently identified a nonsense mutation in *MCT8* causing X-linked leukoencephalopathy in a family from only two affected male samples (24). We have also identified two possible but inconclusive missense variants (*L1CAM* and *TMEM187*) in a family with an atypical X-linked leukodystrophy from only two affected male samples (25). In this study, exome sequencing accompanied by appropriate bioinformatics techniques and a co-segregation evaluation successfully revealed a disease-causing mutation in *OFD1*, which could not have been assumed to be a candidate based on the clinical manifestations of the affected male patients. Unbiased rapid screening through these technologies is a powerful method for the detection of mutations in unexpected causative genes in undiagnosed patients with multiple congenital malformations.

In conclusion, we have identified a causative splicing mutation in *OFD1*, through exome sequencing, in a family with three males having an 'unclassified' X-linked lethal congenital malformation syndrome. The affected males manifested severe multisystem complications in addition to the cardinal features of OFD1 and the carrier female showed only subtle features of OFD1. The present patients, as well as the previously reported male patients from four families (one with clinical OFD1; one with SGBS2 and an *OFD1* mutation; two with JBTS10 and *OFD1* mutations), would belong to a single syndrome spectrum caused by truncating *OFD1* mutations, presenting with craniofacial features (macrocephaly, depressed or broad nasal bridge, and lip abnormalities), postaxial polydactyly, respiratory insufficiency with recurrent respiratory tract infections in survivors, severe mental or developmental retardation, and brain malformations (hypoplasia or agenesis of corpus callosum and/or cerebellar vermis and posterior fossa abnormalities).

Acknowledgements

The authors are grateful to the family for their participation in this study. The authors are also thankful to Prof Germana Meroni (Cluster in Biomedicine, Trieste) for mutation analysis of *MID1*, Dr Takeshi Futatani (Department of Pediatrics, Toyama Prefectural Central Hospital, Toyama, Japan), Dr Masahiko Kawabata (Department of Internal Medicine, Toyama Prefectural Central Hospital, Toyama, Japan), and Dr Akio Uchiyama (Department of Pathology, Toyama Prefectural Central Hospital, Toyama, Japan) for collecting clinical information; Dr Gen Nishimura (Department of Radiology, Tokyo Metropolitan Children's Medical Center) for helping radiological assessment; and Miss Junko Kunimi (Department of Medical Genetics, Shinshu University School of Medicine, Matsumoto, Japan) and Dr Shin-ya Nishio (Department of Otolaryngology, Shinshu University School of Medicine, Matsumoto, Japan) for their technical assistance. This work was supported by research grants from the Ministry of Health, Labour and Welfare (T. K., Y. F., H. S., N. Mi., and N. Ma.), the Japan Science and Technology Agency (N. Ma.), the Strategic Research Program for Brain Sciences (N. Ma.) and a Grant-in-Aid for Scientific Research on Innovative Areas (Foundation of Synapse and Neurocircuit Pathology) from the Ministry of Education, Culture, Sports, Science and Technology of Japan (N. Ma.), a Grant-in-Aid for Scientific Research from Japan Society for the Promotion of Science (N. Ma.), a Grant-in-Aid for Young Scientist from Japan Society for the Promotion of Science (H. S. and N. Mi.) and a grant from the Takeda Science Foundation (N. Mi. and N. Ma.). This work was performed at the Advanced Medical Research Center, Yokohama City University, Japan.

Y. T., H. D., H. S., and N. Mi. performed the genetic analysis; T. K., K. H., Y. N., K. W., and Y. F. evaluated clinical aspects of the family, recruited samples, and prepared them for the analysis. Y. T., T. K. and N. Ma. wrote the manuscript.

Ethics approval

The work was approved by the Yokohama City University (Faculty of Medicine) and the Shinshu University (School of Medicine). Patient consent was obtained.

References

1. Papillon-Leage M, Psaume J. Une malformation hereditaire de la muquese buccale: brides et freins anomaux. Rev Stomatol 1954: 55: 209–227.
2. Gorlin RJ, Psaume J. Orofaciodigital dysostosis: a new syndrome. A study of 22 cases. J Pediatr 1962: 61: 520–530.
3. Ferrante MI, Giorgio G, Feather SA et al. Identification of the gene for oral-facial-digital type I syndrome. Am J Hum Genet 2001: 68: 569–576.
4. Macca M, Franco B. The molecular basis of oral-facial-digital syndrome, type 1. Am J Med Genet C 2009: 151C: 318–325.
5. Toriello HV, Franco B. Oral-facial-digital syndrome type I. In: Pagon RA, Bind TD, Dolan CR, Stephans K, Adam MP, eds. GeneReviews at genetests: Medical Genetics Information Resource (database online). Seattle, WA: Copyright, University of Washington, 1993–2011, from http://www.genetests.org. Accessed on July 23, 2011.
6. Morleo M, Franco B. Dosage compensation of the mammalian X-chromosome influences the phenotypic variability of X-linked dominant male-lethal disorders. J Med Genet 2008: 45: 401–408.
7. Goodship J, Platt J, Smith R, Burn J. A male with type I orofaciodigital syndrome. J Med Genet 1991: 28: 691–694.
8. Fontanella B, Russolillo G, Meroni G. MID1 mutations in patients with X-linked Opitz G/BBB syndrome. Hum Mutat 2008: 29: 584–594.
9. Nishimura-Tadaki A, Wada T, Bano G et al. Breakpoint determination of X;autosome balanced translocations in four patients with premature ovarian failure. J Hum Genet 2011: 56: 156–160.
10. Budny B, Chen W, Omran H et al. A novel X-linked recessive mental retardation syndrome comprising macrocephaly and ciliary dysfunction is allelic to oral-facial-digital type I syndrome. Hum Genet 2006: 120: 171–178.
11. Terespolsky D, Farrell SA, Siegel-Bartelt J, Weksberg R. Infantile lethal variant of Simpson-Golabi-Behmel syndrome associated with hydrops fetalis. Am J Med Genet 1995: 59: 329–333.
12. Brzustowicz LM, Farrell S, Khan MB, Weksberg R. Mapping of a new SGBS locus to chromosome Xp22 in a family with a severe form of Simpson-Golabi-Behmel syndrome. Am J Hum Genet 1999: 65: 779–783.
13. Coene KL, Roepman R, Doherty D et al. OFD1 is mutated in X-linked Joubert syndrome and interacts with LCA5-encoded lebercilin. Am J Hum Genet 2009: 85: 465–481.
14. McGraw P. The molar tooth sign. Radiology 2002: 229: 671–672.
15. Chance PF, Cavalier L, Satran D, Pellegrino JE, Koenig M, Dobyns WB. Clinical nosologic and genetic aspects of Joubert and related syndromes. J Child Neurol 1999: 14: 660–666.

16. Sartori S, Ludwig K, Fortuna M et al. Dandy-Walker malformation masking the molar tooth sign: an illustrative case with magnetic resonance imaging follow-up. J Child Neurol 2010: 25: 1419–1422.
17. Barkovich AJ. Anomalies with cerebellar dysgenesis: vermian dysgenesis. In: Barkovich AJ, ed. Pediatric neuroimaging, 4th edn. Lippincott Williams & Wilkins, Philadelphia 2005: 391–396.
18. Brancati F, Dallapiccola B, Valente EM. Joubert syndrome and related disorders. Orphanet J Rare Dis 2010: 5: 20.
19. Prattichizzo C, Macca M, Novelli V et al. Mutational spectrum of the oral-facial-digital type I syndrome: a study on a large collection of patients. Hum Mutat 2008: 29: 1237–1246.
20. Thauvin-Robinet C, Cossée M, Cormier-Daire V et al. Clinical, molecular, and genotype-penotype correlation studies from 25 cases of oral-facial-digital syndrome type 1: a French and Belgian collaborative study. J Med Genet 2006: 43: 54–61.
21. Thauvin-Robinet C, Franco B, Saugier-Veber P et al. Genomic deletions of *OFD1* account for 23% of oral-facial-digital type 1 syndrome after negative DNA sequencing. Hum Mutat 2008: 30: E320–E329.
22. Shendure J, Ji H. Next-generation DNA sequencing. Nat Biotechnol 2008: 26: 1135–1145.
23. Bamshad MJ, Ng SB, Bigham AW et al. Exome sequencing as a tool for Mendelian disease gene discovery. Nat Rev Genet 2011: 12: 745–755.
24. Tsurusaki Y, Osaka H, Hamanoue H et al. Rapid detection of a mutation causing X-linked leukodystrophy by exome sequencing. J Med Genet 2011: 48: 606–609.
25. Tsurusaki Y, Okamoto N, Suzuki Y et al. Exome sequencing of two patients in a family with atypical X-linked leukodystrophy. Clin Genet 2011: 80: 161–166.

Neurogenetics
DOI 10.1007/s10048-012-0337-6

SHORT COMMUNICATION

A *DYNC1H1* mutation causes a dominant spinal muscular atrophy with lower extremity predominance

Yoshinori Tsurusaki · Shinji Saitoh · Kazuhiro Tomizawa · Akira Sudo · Naoko Asahina · Hideaki Shiraishi · Jun-ichi Ito · Hajime Tanaka · Hiroshi Doi · Hirotomo Saitsu · Noriko Miyake · Naomichi Matsumoto

Received: 24 February 2012 / Accepted: 3 July 2012

Abstract Whole-exome sequencing of two affected sibs and their mother who showed a unique quadriceps-dominant form of neurogenic muscular atrophy disclosed a heterozygous *DYNC1H1* mutation [p.H306R (c.917A>G)]. The identical mutation was recently reported in a pedigree with the axonal form of Charcot–Marie–Tooth disease. Three other missense mutations in *DYNC1H1* were also identified in families with dominant spinal muscular atrophy with lower extremity predominance. Their clinical features were consistent with those of our family. Our study has demonstrated that the same *DYNC1H1* mutation could cause spinal muscular atrophy as well as distal neuropathy, indicating pleotropic effects of the mutation.

Keywords Spinal muscular atrophy with lower extremity predominance · DYNC1H1 · Whole-exome sequencing · Charcot–Marie–Tooth disease · Allelic disease

Introduction

DYNC1H1 encodes cytoplasmic dynein heavy chain 1, which is a subunit of the primary motor protein responsible for retrograde axonal transport in neurons [1]. Weedon et al. first identified a missense mutation [p.H306R (c.917A>G)] of *DYNC1H1* in a large family with axonal Charcot–Marie–Tooth (CMT) disease by using exome sequencing, indicating the significance of *DYNC1H1* in the peripheral nerve axon [2]. Subsequently, Harms et al. reported three other missense mutations in the tail domain of *DYNC1H1* in families with dominant spinal muscular atrophy with lower extremity predominance (SMA-LED, OMIM 158600), expanding the role of *DYNC1H1* to maintenance of motor neuron itself [3]. Recently, two de novo missense mutations have also been identified in patients with severe intellectual disability and variable neuronal migration defects [4].

Authorship Y.T. and S.S. contributed equally to this work.

Y. Tsurusaki · H. Doi · H. Saitsu · N. Miyake · N. Matsumoto (✉)
Department of Human Genetics, Yokohama City University Graduate School of Medicine,
3-9 Fukuura, Kanazawa-ku,
Yokohama 236-0004, Japan
e-mail: naomat@yokohama-cu.ac.jp

S. Saitoh (✉)
Department of Pediatrics and Neonatology, Graduate School of Medical Sciences, Nagoya City University,
Kawasumi-1, Mizuho-cho, Mizuho-ku,
Nagoya 467-8601, Japan
e-mail: ss11@med.nagoya-cu.ac.jp

K. Tomizawa
Department of Pediatrics, Nakashibetsu Town Hospital,
Nakashibetsu, Japan

A. Sudo
Department of Pediatrics, Sapporo City General Hospital,
Sapporo, Japan

N. Asahina · H. Shiraishi
Department of Pediatrics, Hokkaido University Graduate School of Medicine,
Sapporo, Japan

J.-i. Ito
Department of Pediatrics, Taiyo no Sono,
Date, Japan

H. Tanaka
Department of Pediatrics, Asahikawa Habilitation Center for Disabled Children,
Asahikawa, Japan

Published online: 31 July 2012

Therefore, *DNYC1H1* may have broad biological effects on development and maintenance of the nervous system.

In this study, we describe a family containing three individuals with dominant spinal muscular atrophy with lower extremity predominance. Exome sequencing identified an identical *DYNC1H1* mutation found in a pedigree with axonal CMT [2], demonstrating the pleotropic effects of the *DYNC1H1* mutation.

Subjects and methods

Subjects

Patient 1 This female patient was born after 41 weeks of gestation. Pregnancy was uneventful. Birth weight was 3,080 g. Her initial development was normal, and head control was recognized at 3–4 months. Late infantile motor development was mildly delayed, and she could walk unassisted at 1 year and 8 months. Unstable gait persisted thereafter, and she was referred to us at 3 years and 1 month of age for evaluation. On examination, proximal lower limb-dominant muscle atrophy and decreased deep tendon reflex were noted. Gower's sign was positive. No other neurological deficits were demonstrated. No sensory disturbance or ataxia was present.

The following examinations were performed at 3 years and 1 month of age. Neither serum transaminase nor creatine kinase was elevated. Motor nerve conduction velocity was within the normal limits (55.8 m/s for the right tibial nerve). Brain MRI revealed normal findings. Muscle computed tomography (CT) demonstrated severe atrophy and lipid degeneration, predominantly in the bilateral quadriceps femoris muscle (Fig. 1). The upper limbs and distal lower limbs were not affected. A muscle biopsy from the quadriceps femoris muscle demonstrated severe grouping atrophy of type 2 fibers with a massive increase in the amount of fibrous tissue and sparse enlarged type 1 fibers (Fig. 2).

The patient is currently 18 years old and graduated from regular high school. Her motor development has steadily progressed, and she only shows moderate proximal lower limb-dominant muscle weakness and atrophy. She can walk unassisted and shows a waddling gait and positive Gower's sign. No sensory disturbance or ataxia is noted. She does not have any intellectual disability.

Patient 2 Patient 2 is the half brother of patient 1. He was born after 38 weeks of gestation to the same mother and a different father from patient 1's. His birth weight was 2,405 g. He could control his head at 3–4 months, turn over at 6 months, and sit unassisted at 7–8 months. His motor development was delayed thereafter, and he walked unassisted at 1 year and 7 months. His mental development was normal. Because of a persistently unstable gait, he was hospitalized and examined at 5 years and 11 months. Physical examination revealed moderate muscle weakness in the proximal lower limb, but Gower's sign was negative. Deep tendon reflex was normal. No sensory disturbance or ataxia was recognized. Ankle joint contracture and foot deformity were absent.

The following examinations were performed at 5 years and 11 months of age. Serum transaminase and creatine kinase levels were normal. Brain and spinal MRI revealed no abnormal findings. Motor nerve conduction velocity and amplitude were within the normal limits (51.1 m/s, 4.6 mV for the right median nerve, 51.1 m/s, 9.9 mV for the right tibial nerve). Sensory nerve conduction velocity and amplitude were also within the normal limits (57.3 m/s, 28.4 uV for the right median nerve, 63.7 m/s, 9.6 uV for the right sural nerve). Needle electromyography of the anterior tibial muscle showed long high-amplitude discharges (3.5–4.0 mV, 10 ms) consistent with a neurogenic pattern, although no denervation potential, including positive sharp wave or fibrillation potential, was present, while the right biceps brachii showed inconclusive results. Muscle CT revealed severe atrophy and lipid degeneration, most predominantly in the bilateral quadriceps femoris. The upper limbs and distal lower limbs were not affected (Fig. 1).

The patient is now 12 years old and can walk unassisted but with a waddling gait. He has shown no further deterioration of motor function. Proximal lower limb weakness and wasting are evident, but the patient shows no upper limb weakness. No sensory disturbance or ataxia has been recognized.

Patient 3 Patient 3 is the mother of the two sibs. She is currently 50 years of age. No family history (except for her children) of neuromuscular disorders was noted. Until we examined the second sib, she had not been noted to have proximal lower limb muscle weakness. She did not recall her infantile development, and it was impossible to obtain further information. She graduated from a regular high school, married, and raised her children. She has not shown any neurological deterioration. She did not show a waddling gait, but had difficulty squatting. She was examined at 44 years of age. Her deep tendon reflex was normal, and no ankle joint contracture was present. Muscle CT revealed bilateral quadriceps-dominant muscle atrophy and lipid degeneration (Fig. 1). She also demonstrated mild muscle atrophy in her hip. Unfortunately, CT of the distal lower limb muscle could not be performed.

Exome sequencing

We performed the whole-exome sequencing of two patients (II-1 and II-2; Fig. 3a). Three micrograms of genomic DNA

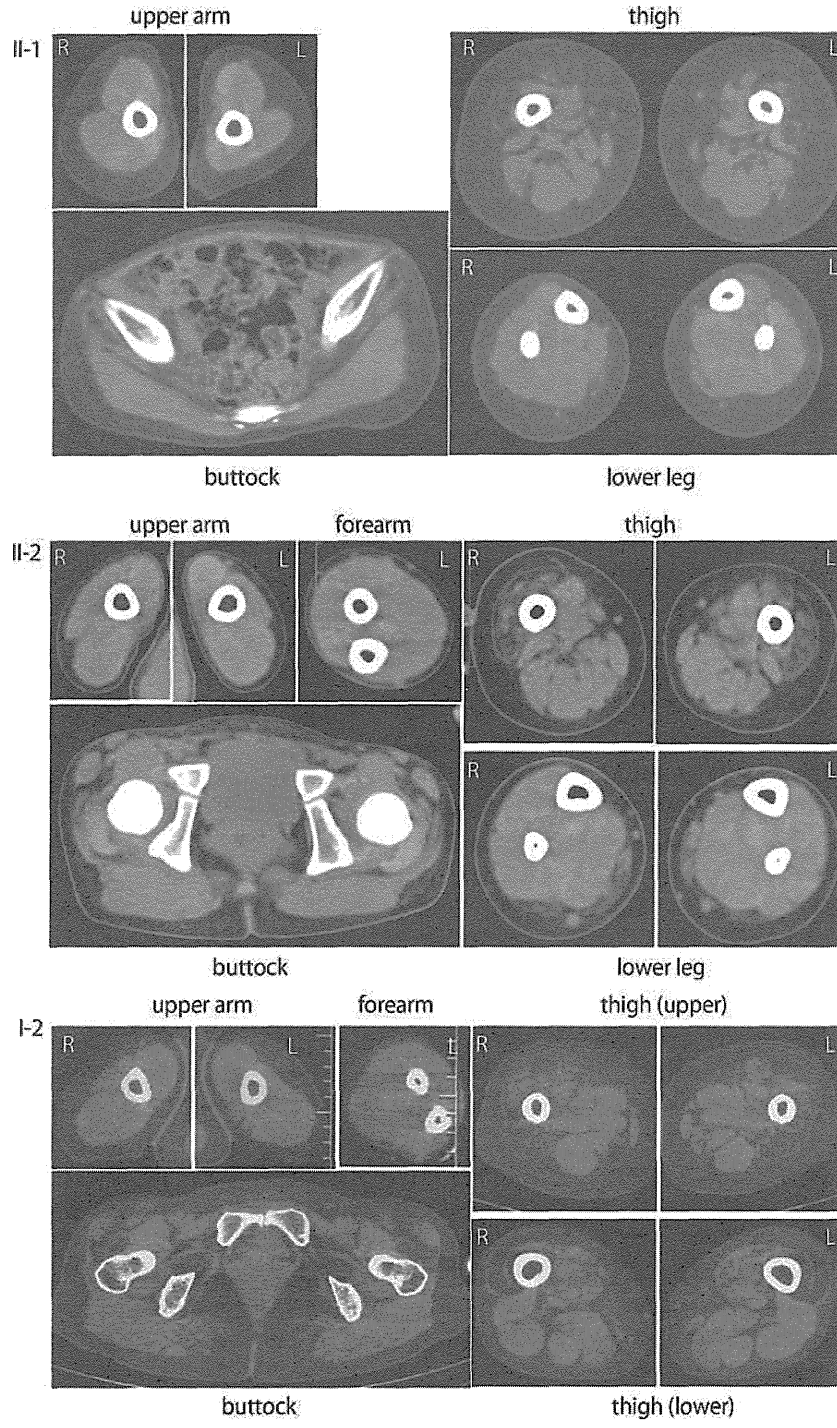

Fig. 1 Muscle imaging. Muscle computed tomography images of patient II-1 at the age of 3 years and 1 month (*upper*), patient II-2 at the age of 5 years and 11 months (*middle*), and patient I-1 at the age of 44 years (*lower*) are displayed. *R* right, *L* left

was processed using a SureSelect Human All Exon Kit v.1 (approximately 180,000 exons covering 38 Mb of the CCDS database) (Agilent Technologies, Santa Clara, CA) according to the manufacturer's protocol. Captured DNA was diluted to a concentration of 8 pM and sequenced on a Genome Analyzer IIx (Illumina, San Diego, CA) with 76-bp paired-end reads. We used two of the eight lanes in the flow cell (Illumina). Image analyses and base calling were performed by sequence control software real-time analysis and/or Off-line Basecaller software v1.6.0 (Illumina). Alignment was performed using CASAVA software v1.6.0. The quality-controlled (Path Filter) reads were mapped to the human reference genome (UCSC hg19, NCBI build 37), using mapping and assembly with quality (MAQ) and NextGENe software v2.0 (SoftGenetics, State College, PA). SNPs in MAQ-passed reads were annotated using the

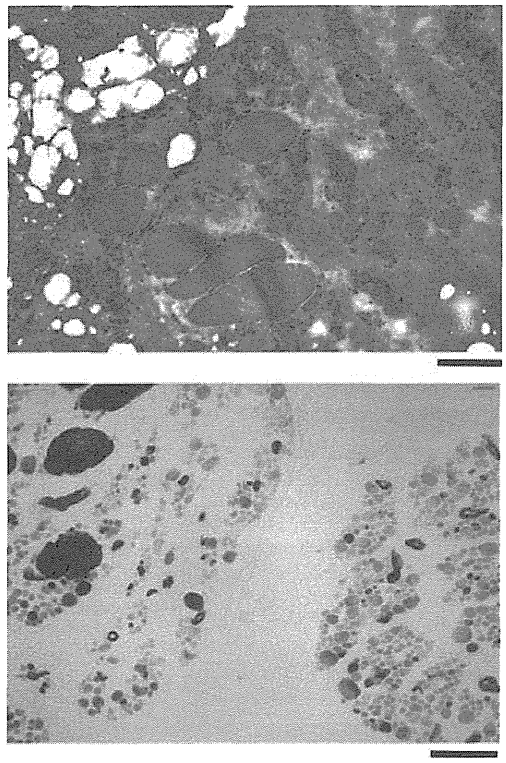

Fig. 2 Histological study. Hematoxylin–eosin staining (*upper*) and ATPase staining (pH=4.6, *lower*) of the quadriceps femoris muscle of patient II-1. The *scale bar* indicates 100 μm in length

SeattleSeq Annotation website (http://gvs.gs.washington.edu/SeattleSeqAnnotation/).

Priority scheme and capillary sequencing

We adopted a prioritization scheme used in recent studies to identify the pathogenic mutation [5–7]. Called variants found by each informatics method filtered into unregistered variants (excluding registered dbSNP131 and 1,000 genomes), overlapping variants called in common by NextGENe and MAQ, nonsynonymous changes (NS), splice site mutations (±2 bp from the exon–intron junctions) (SS), small insertions or deletions (indels), and overlapping variants called in II-1 and II-2 were checked, and variants found in our 33 in-house exomes derived from 19 healthy individuals and 14 individuals with unrelated diseases were excluded (Table 1). An online human genome mutation database (HGMD, https://portal.biobase-international.com/hgmd/pro/start.php) was referred to as a reference for disease-causing mutations. The variants were confirmed as true positives by Sanger sequencing of polymerase chain reaction products amplified using genomic DNA as a template. Sanger sequencing was performed on an ABI3500XL or ABI3100 autosequencer (Life Technologies, Carlsbad, CA). Sequencing data were analyzed using Sequencer software (Gene Codes Corporation, Ann Arbor, MI).

A total of 177 Japanese control samples (354 alleles) were check by high-resolution melting analysis using a LightCycler 480 (Roche Diagnostics, Otsu, Japan) to see the variant frequency. The reaction was performed in 10 μl containing 10 ng of genomic DNA, 0.2 mM dNTPs,

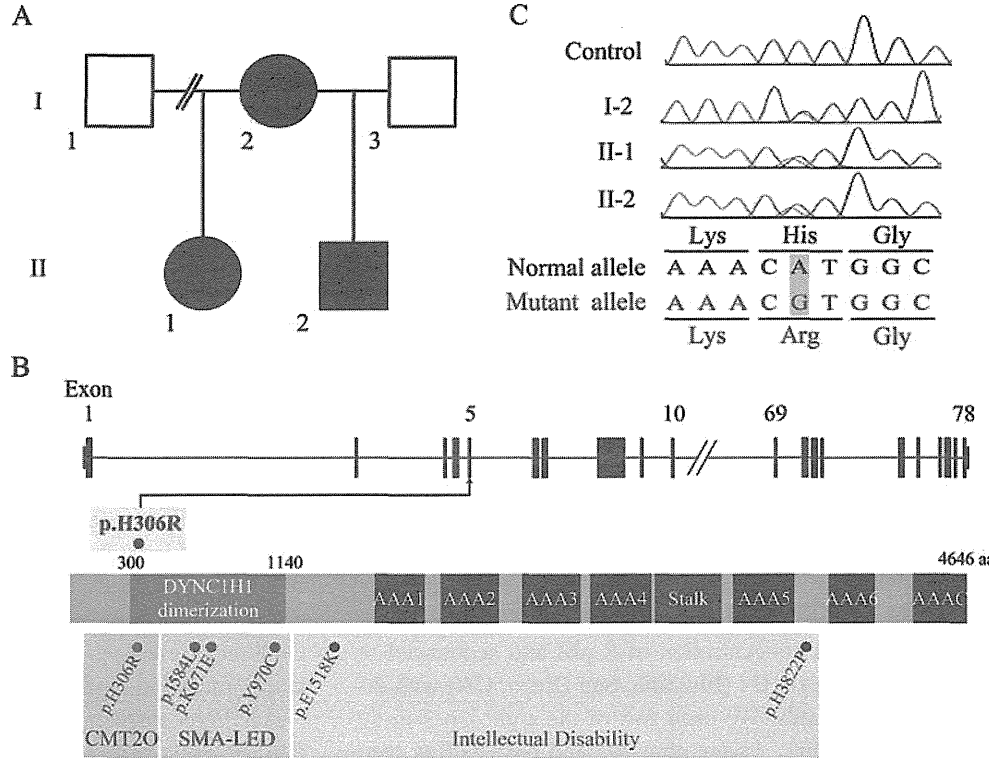

Fig. 3 Genetic study. **a** Familial pedigree. **b** The gene structure of *DYNC1H1* with the mutation [p.H306R (c.917A>G)] (*upper*), the protein structure with functional domains (*middle*), and reported mutations corresponding to respective diseases (*lower*). *AAA* ATPase domains (AAA 1 to 6), *AAAC* unrelated seventh domain. **c** Sequences of a control and the family members are displayed. Heterozygous mutations are observed in patients I-2, II-1, and II-2

Table 1 Variant priority scheme of exome sequencing data

	Half sister		Half brother	
	NextGENe	MAQ (SeattleSeq)	NextGENe	MAQ (SeattleSeq)
Total variants called	73,966	174,757	73,370	163,707
Autosomal+chr X	71,522	174,165	70,068	163,013
Unknown SNP variants (dbSNP, 1,000 genomes)	11,132	21,284	10,857	19,858
Overlap of NextGENe and MAQ	1,598		1,482	
NS/SS/I	426		411	
Overlapping in half sibs	135			
Unknown variants (in-house database)	62			

MAQs were annotated using SeattleSeq annotation. The annotation includes gene names, dbSNP rs IDs, and SNP functions (e.g., missense), protein positions and amino acid changes. *NS* nonsynonymous, *SS* splice site (±2 bp), *I* indels

0.125 U of ExTaq (Takara Bio, Inc., Otsu, Japan), 1× buffer, and 1.5 μM SYTO9 (Invitrogen, Carlsbad, CA).

Results

Approximately 9.8 and 9.5 Gb of sequence data were generated for II-1 and II-2, respectively. This approach resulted in more than 85.8 % (II-1) and 86.5 % (II-2) of the target regions being covered by ten reads or more. Two informatics methods identified 62 potentially pathogenic changes (Table 1). We found a missense mutation [p.H306R (c.917A>G)] in *DYNC1H1* from among 62 variants using the HGMD as a reference; this mutation has been reported as a causative mutation for CMT disease [2]. The heterozygous missense mutation was confirmed in I-2, II-1, and II-2 (Fig. 3b). This missense mutation was not found in 177 control samples.

Discussion

The identical *DYNC1H1* mutation (p.H306R) found in a large pedigree with axonal type of CMT disease was detected by exome sequencing in a family with a unique form of quadriceps-dominant neurogenic muscular atrophy [2]. Three members of the family demonstrated very similar clinical features, which were distinct from CMT disease. The most striking feature was a unique distribution of muscle involvement. The quadriceps femoris muscle was almost selectively involved in the early course of the disease, and the proximal lower limb was predominantly involved throughout the disease course. Recently, three other missense mutations were detected in families with SMA-LED. Clinical features of the current family are essentially consistent with those of SMA-LED, hallmarks of which are early childhood onset of proximal leg weakness with muscle atrophy and nonlength-dependent motor neuron disease without sensory involvement [3]. Nonprogressive clinical course despite early childhood onset as in our family should be another hallmark of SMA-LED. These cumulative data clearly indicate that *DYNC1H1* plays an essential role in maintenance of spinal motor neurons and their axon.

Thus far, four missense mutations (p.H306R, p.I584L, p.K671E, p.Y970C) identified in human cases of CMT or SMA-LED are located in the same tail domain for DYNC1H1 dimerization. It is of note that three missense mutations (p.F580Y, p.G1042A, p.T1057C) found in mouse models are also located in the tail domain [8–10]. These mice involve not only spinal motor neurons but also sensory and cortical neurons. The tail domain is thought to be essential for dimerization of dynein heavy chains, and thus, missense mutations in the tail domain may disrupt function of dynein complex formation in a dominant negative manner. Two distinct de novo mutations (p.E1518K, p.H3822P) identified in patients with severe intellectual disability and variable neuronal migration defects were located outside of the tail domain. These patients also showed possible peripheral nerve involvement, but formal neurophysiological investigation was not available. Since mice with *Dync1h1* abnormality show broad central nervous system involvement, *DNYC1H1* is likely to cause a wide range of neuronal migration disorders.

CMT disease with the p.H306R mutation has been designated as CMT2O (OMIM 614228). Most members of the pedigree with p.H306R reported by Weedon et al. demonstrated distal dominant muscle weakness, while one patient showed proximal lower limb-dominant muscle atrophy as in our family [2]. Therefore, the same missense mutation in the tail domain could cause CMT2O phenotype and SMA-LED phenotype even within the same pedigree. It is hard to explain the underlying mechanism of pleotropic effects of the mutation. Further studies are absolutely necessary to elucidate phenotype–genotype correlation and pleiotropic mutational consequences.

Acknowledgments We would like to thank the family for their participation in this study. This work was supported by research grants from the Ministry of Health, Labour and Welfare (H.S., N. Miyake, and

N. Matsumoto); a Grant-in-Aid for Scientific Research from the Japan Society for the Promotion of Science (N. Miyake and N. Matsumoto); a grant from the Japan Science and Technology Agency (N. Matsumoto), the Strategic Research Program for Brain Sciences (N. Matsumoto); a Grant-in-Aid for Scientific Research on Innovative Areas (Foundation of Synapse and Neurocircuit Pathology) from the Ministry of Education, Culture, Sports, Science and Technology of Japan (N. Matsumoto); a research grant from Naito Foundation (N. Matsumoto); and research grants from Takeda Science Foundation (N. Miyake and N. Matsumoto). This work was performed at the Advanced Medical Research Center, Yokohama City University, Japan.

References

1. Pfister KK, Shah PR, Hummerich H, Russ A, Cotton J, Annuar AA, King SM, Fisher EM (2006) Genetic analysis of the cytoplasmic dynein subunit families. PLoS Genet 2(1):e1. doi:10.1371/journal.pgen.0020001
2. Weedon MN, Hastings R, Caswell R, Xie W, Paszkiewicz K, Antoniadi T, Williams M, King C, Greenhalgh L, Newbury-Ecob R, Ellard S (2011) Exome sequencing identifies a DYNC1H1 mutation in a large pedigree with dominant axonal Charcot–Marie–Tooth disease. Am J Hum Genet 89(2):308–312. doi:10.1016/j.ajhg.2011.07.002
3. Harms MB, Ori-McKenney KM, Scoto M, Tuck EP, Bell S, Ma D, Masi S, Allred P, Al-Lozi M, Reilly MM, Miller LJ, Jani-Acsadi A, Pestronk A, Shy ME, Muntoni F, Vallee RB, Baloh RH (2012) Mutations in the tail domain of DYNC1H1 cause dominant spinal muscular atrophy. Neurology 78(22):1714–1720. doi:10.1212/WNL.0b013e3182556c05
4. Willemsen MH, Vissers LE, Willemsen MA, van Bon BW, Kroes T, de Ligt J, de Vries BB, Schoots J, Lugtenberg D, Hamel BC, van Bokhoven H, Brunner HG, Veltman JA, Kleefstra T (2012) Mutations in DYNC1H1 cause severe intellectual disability with neuronal migration defects. J Med Genet 49(3):179–183. doi:10.1136/jmedgenet-2011-100542
5. Tsurusaki Y, Okamoto N, Suzuki Y, Doi H, Saitsu H, Miyake N, Matsumoto N (2011) Exome sequencing of two patients in a family with atypical X-linked leukodystrophy. Clin Genet 80 (2):161–166. doi:10.1111/j.1399-0004.2011.01721.x
6. Saitsu H, Osaka H, Sasaki M, Takanashi J, Hamada K, Yamashita A, Shibayama H, Shiina M, Kondo Y, Nishiyama K, Tsurusaki Y, Miyake N, Doi H, Ogata K, Inoue K, Matsumoto N (2011) Mutations in POLR3A and POLR3B encoding RNA polymerase III subunits cause an autosomal-recessive hypomyelinating leukoencephalopathy. Am J Hum Genet 89(5):644–651. doi:10.1016/j.ajhg.2011.10.003
7. Doi H, Yoshida K, Yasuda T, Fukuda M, Fukuda Y, Morita H, Ikeda S, Kato R, Tsurusaki Y, Miyake N, Saitsu H, Sakai H, Miyatake S, Shiina M, Nukina N, Koyano S, Tsuji S, Kuroiwa Y, Matsumoto N (2011) Exome sequencing reveals a homozygous SYT14 mutation in adult-onset, autosomal-recessive spinocerebellar ataxia with psychomotor retardation. Am J Hum Genet 89 (2):320–327. doi:10.1016/j.ajhg.2011.07.012
8. Hafezparast M, Klocke R, Ruhrberg C, Marquardt A, Ahmad-Annuar A, Bowen S, Lalli G, Witherden AS, Hummerich H, Nicholson S, Morgan PJ, Oozageer R, Priestley JV, Averill S, King VR, Ball S, Peters J, Toda T, Yamamoto A, Hiraoka Y, Augustin M, Korthaus D, Wattler S, Wabnitz P, Dickneite C, Lampel S, Boehme F, Peraus G, Popp A, Rudelius M, Schlegel J, Fuchs H, Hrabe de Angelis M, Schiavo G, Shima DT, Russ AP, Stumm G, Martin JE, Fisher EM (2003) Mutations in dynein link motor neuron degeneration to defects in retrograde transport. Science 300(5620):808–812. doi:10.1126/science.1083129
9. Chen XJ, Levedakou EN, Millen KJ, Wollmann RL, Soliven B, Popko B (2007) Proprioceptive sensory neuropathy in mice with a mutation in the cytoplasmic dynein heavy chain 1 gene. J Neurosci 27(52):14515–14524. doi:10.1523/JNEUROSCI.4338-07.2007
10. Ori-McKenney KM, Vallee RB (2011) Neuronal migration defects in the Loa dynein mutant mouse. Neural Dev 6:26. doi:10.1186/1749-8104-6-26

Journal of Human Genetics (2013) 58, 113–115

www.nature.com/jhg

SHORT COMMUNICATION

The diagnostic utility of exome sequencing in Joubert syndrome and related disorders

Yoshinori Tsurusaki[1], Yasuko Kobayashi[2], Masataka Hisano[3], Shuichi Ito[4], Hiroshi Doi[1], Mitsuko Nakashima[1], Hirotomo Saitsu[1], Naomichi Matsumoto[1] and Noriko Miyake[1]

Joubert syndrome (JS) and related disorders (JSRD) are autosomal recessive and X-linked disorders characterized by hypoplasia of the cerebellar vermis with a characteristic 'molar tooth sign' on brain imaging and accompanying neurological symptoms including episodic hyperpnoea, abnormal eye movements, ataxia and intellectual disability. JSRD are clinically and genetically heterogeneous, and, to date, a total of 17 causative genes are known. We applied whole-exome sequencing (WES) to five JSRD families and found mutations in all: either *CEP290*, *TMEM67* or *INPP5E* was mutated. Compared with conventional Sanger sequencing, WES appears to be advantageous with regard to speed and cost, supporting its potential utility in molecular diagnosis.
Journal of Human Genetics (2013) **58,** 113–115; doi:10.1038/jhg.2012.117; published online 4 October 2012

Keywords: *CEP290*; exome sequencing; *INPP5E*; Joubert syndrome; molecular diagnosis; *TMEM67*

Joubert syndrome (JS) and related disorders (JSRD) are autosomal recessive and X-linked disorders characterized by hypoplasia of the cerebellar vermis with the characteristic neuroradiological 'molar tooth sign' and accompanying neurological symptoms including dysregulation of breathing pattern, ataxia and developmental delay. JSRD are classified into six subtypes: pure JS, JS with ocular defect, JS with renal defect, JS with oculorenal defects, JS with hepatic defect and JS with orofaciodigital defects.[1] To date, 17 causative genes have been identified in JSRD: *INPP5E*,[2] *TMEM216*,[3] *AHI1*,[4] *NPHP1*,[5] *CEP290*,[6] *TMEM67*,[7] *RPGRIP1L*,[8] *ARL13B*,[9] *CC2D2A*,[10] *OFD1*,[11] *TTC21B*,[12] *KIF7*,[13] *TCTN1*,[14] *TMEM237*,[15] *CEP41*,[16] *TMEM138*,[17] and *C5ORF42*.[18] Because of the clinical and genetic heterogeneity in JSRD, it can be very difficult to identify the causative mutations in individual cases.

We encountered five non-consanguineous Japanese families with JSRD (Figure 1a) and molar tooth sign was observed in all patients (Figures 1b–e, Supplementary Table 1). Peripheral blood samples were obtained from patients and their family members after written informed consent was given. To identify causative mutations, we performed whole-exome sequencing (WES) in five probands of the five families (one proband from each family). DNA was processed using the SureSelectXT Human All Exon 50 Mb library or V4 (51 Mb) library (Agilent Technologies, Santa Clara, CA, USA), and sequenced on a Genome Analyzer IIx sequencer (Illumina, San Diego, CA, USA) with 108 bp paired-end reads, or on a HiSeq2000 sequencer (Illumina) with 101 bp paired-end reads and 7 bp index reads. Image analysis and base calling were performed by Illumina pipeline. Approximately 3.8–6.0 Gb of sequence data were mapped to the human reference genome (GRCh37.1/hg19) with Novoalign or Burrows-Wheeler Aligner. The mean depth of coverage was 55–125 reads, with 88–96% of all coding exons being covered by 5 × or more reads.

Out of all variants within exons and ± 20-bp intronic regions from the exon–intron boundaries, those registered in dbSNP135, 1000 Genomes and ESP5400 and located within the segmental duplications were removed. Homozygous or compound heterozygous variants of 17 JSRD causative genes were then picked up. In patients 1, 2, 3 and 4 whose DNA was captured by the SureSelectXT Human All Exon 50 Mb library, ~90% of the entire coding regions in 13 of 17 causative genes were covered by 5 × reads or more. In patient 5 captured by the V4 (51 Mb) library, >90% of the coding region was covered by 5 × reads or more (Supplementary Table 2), indicating that the V4 library offered superior coverage to the SureSelectXT library around the regions of the JSRD genes.

All patients from the five families possessed novel compound heterozygous mutations or a homozygous mutation in known genes later confirmed by Sanger sequencing (Figure 1a): c.1862G>A (p.R621Q)/c.700dupC (p.L234Pfs*56) in *INPP5E* (9q34.3) for family 1; c.5788A>T (p.K1930*)/c.6012-12A>T in *CEP290* (12q21.32) for family 2; c.329A>G (p.D110G)/c.2322 + 5delG in *TMEM67* (8q22.1) for family 3; homozygous c.6012-12A>T in *CEP290* for family 4; and c.214G>T (p.E72*)/c.6012-12A>T in *CEP290* for family 5. No other variants within 17 known genes have been identified after excluding

[1]Department of Human Genetics, Yokohama City University Graduate School of Medicine, Yokohama, Japan; [2]Department of Pediatrics, Gunma University Graduate School of Medicine, Maebashi, Japan; [3]Department of Nephrology, Chiba Children's Hospital, Chiba, Japan and [4]National Center for Child Health and Development, Tokyo, Japan
Correspondence: Dr N Miyake, Department of Human Genetics, Yokohama City University Graduate School of Medicine, 3-9 Fukuura, Kanazawa-ku, Yokohama 236-0004, Japan.
E-mail: nmiyake@yokohama-cu.ac.jp
Received 31 July 2012; revised 3 September 2012; accepted 5 September 2012; published online 4 October 2012

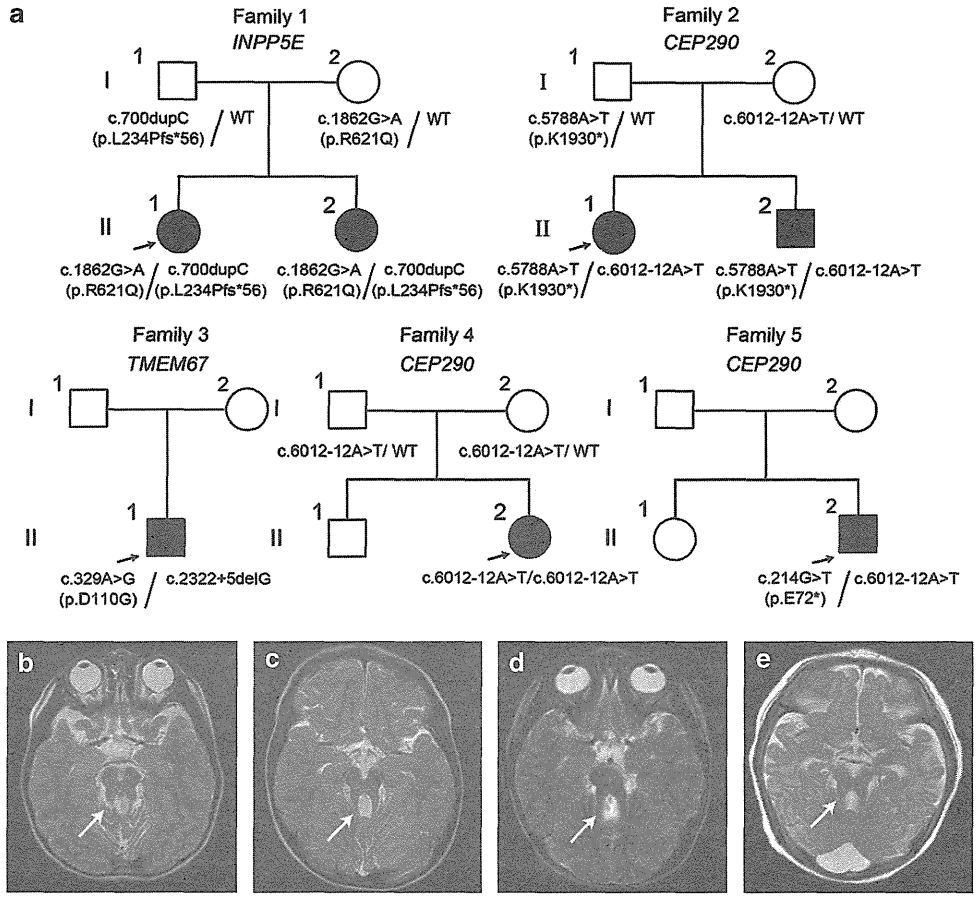

Figure 1 Familial pedigree and brain MRI of the patients. (**a**) JSRD families and mutations. (**b**) T2-weighted axial images of III-1, family 1. (**c**) T2-weighted axial images of III-2, family 1. (**d**) T2-weighted axial images of III-1, family 2. (**e**) T2-weighted axial images of III-2, family 2. The molar tooth sign is visible in all patients (arrowheads).

the variants of dbSNP135, 1000 Genomes and ESP5400. Clinical phenotypes caused by respective mutated genes are discussed in Supplementary text. In families 1, 2 and 4 in which parental samples were available, all parents were heterozygous carriers of one of the mutations. As parental samples were unavailable from families 3 and 5, we determined whether two mutations resided on different alleles by cloning an reverse transcriptase-PCR (RT-PCR) product amplified from total RNA of lymphoblastoid cells into a pCR4-TOPO vector (Life Technologies, Carlsbad, CA, USA) and sequencing. Each mutation was found in a different allele for both families (data not shown). Another variant, c.1894A>G (p.K632E) in *CEP290*, of family 2 was not found to be pathogenic based on web-based analyses such as SIFT, PolyPhen-2 and Mutation Taster (Supplementary Table 3). In families 2, 4 and 5 with a *CEP290* abnormality, c.6012-12A>T was shared. On the basis of our in-house 135 exome data, the allele frequency of the mutation was 1/270 allele (0.74%), indicating that it may be a rare variant in Japanese. The other mutations were not found in our in-house 135 exome data.

Splicing effects were examined in families 3 and 4. RT-PCR was performed on RNA from lymphoblastoid cells of family members using primers spanning exons 42/43 and 45/46 in family 4 and exons 20/21 and 24/25 in family 3 (sequence information available on request). In family 4, only an aberrant cDNA was detected in II-2, whereas the parents (I-1 and I-2) showed two different products including one wild-type, which was detected in a control (Supplementary Figures 1a, b). Sequencing of the mutant product revealed a 57-bp insertion corresponding to the 3′-side of intron 43. As a result, a premature stop codon was introduced at intron 43. In family 3, RT-PCR detected a mutant cDNA in II-1 together with a wild-type product, which was detected in a control. Sequencing of the mutant product confirmed the skipping of exon 22, resulting in an in-frame 27 amino-acid deletion (Supplementary Figures 1c, d).

WES has proved a powerful tool for the identification of novel genes in genetic diseases. It also has tremendous potential for clinical diagnosis and is now being applied in the molecular diagnosis of single-gene disorders such as neurofibromatosis type 1, Marfan syndrome and multi-gene disorders such as retinitis pigmentosa.[19] As shown here, WES would also be suitable for the diagnosis of JSRD, another multi-gene disorder. Though the read-coverage of the old version of SureSelect did not sufficiently collect genomic DNAs for four genes (*INPP5E*, *TMEM216*, *KIF7* and *TCTN1*), the performance of the V4 (51 Mb) library was satisfactory for all genes. Further, as exome capture technology is based on hybridization it can be refractory to homologous regions, so other methods such as multiplex PCR amplification and multiple microdroplet PCR technology could be useful in addition.

In conclusion, we were able to identify causative mutations in five non-consanguineous families with JSRD using WES. The diagnostic utility of WES is obvious, implying that WES or other next-generation sequencing technologies will be a main factor of molecular diagnosis.

ACKNOWLEDGEMENTS

We thank the patients and their families for their participation in this study. This work was supported by research grants from the Ministry of Health, Labor and Welfare (HS, N Matsumoto, N Miyake), the Japan Science and Technology Agency (N Matsumoto), the Strategic Research Program for Brain Sciences (N Matsumoto) and a Grant-in-Aid for Scientific Research on Innovative Areas-(Transcription cycle)-from the Ministry of Education, Culture, Sports, Science and Technology of Japan (N Matsumoto), a Grant-in-Aid for Scientific Research from Japan Society for the Promotion of Science (N Matsumoto), a Grant-in-Aid for Young Scientist from Japan Society for the Promotion of Science (HS, N Miyake) and a grant from the Takeda Science Foundation (N Matsumoto, N Miyake).

Web Resources: The URLs for data presented herein are as follows: Novoalign, http://www.novocraft.com/main/index.php: Burrows-Wheeler Aligner, http://bio-bwa.sourceforge.net/: SIFT, http://sift.jcvi.org/: PolyPhen-2, http://genetics.bwh.harvard.edu/pph2/: Mutation Taster, http://neurocore.charite.de/MutationTaster/

1 Brancati, F., Dallapiccola, B. & Valente, E. M. Joubert Syndrome and related disorders. *Orphanet. J. Rare Dis.* **5,** 20 (2010).
2 Bielas, S. L., Silhavy, J. L., Brancati, F., Kisseleva, M. V., Al-Gazali, L., Sztriha, L. *et al.* Mutations in INPP5E, encoding inositol polyphosphate-5-phosphatase E, link phosphatidyl inositol signaling to the ciliopathies. *Nat. Genet.* **41,** 1032–1036 (2009).
3 Valente, E. M., Logan, C. V., Mougou-Zerelli, S., Lee, J. H., Silhavy, J. L., Brancati, F. *et al.* Mutations in TMEM216 perturb ciliogenesis and cause Joubert, Meckel and related syndromes. *Nat. Genet.* **42,** 619–625 (2010).
4 Ferland, R. J., Eyaid, W., Collura, R. V., Tully, L. D., Hill, R. S., Al-Nouri, D. *et al.* Abnormal cerebellar development and axonal decussation due to mutations in AHI1 in Joubert syndrome. *Nat. Genet.* **36,** 1008–1013 (2004).
5 Parisi, M. A., Bennett, C. L., Eckert, M. L., Dobyns, W. B., Gleeson, J. G., Shaw, D. W. *et al.* The NPHP1 gene deletion associated with juvenile nephronophthisis is present in a subset of individuals with Joubert syndrome. *Am. J. Hum. Genet.* **75,** 82–91 (2004).
6 Valente, E. M., Silhavy, J. L., Brancati, F., Barrano, G., Krishnaswami, S. R., Castori, M. *et al.* Mutations in CEP290, which encodes a centrosomal protein, cause pleiotropic forms of Joubert syndrome. *Nat. Genet.* **38,** 623–625 (2006).
7 Baala, L., Romano, S., Khaddour, R., Saunier, S., Smith, U. M., Audollent, S. *et al.* The Meckel-Gruber syndrome gene, MKS3, is mutated in Joubert syndrome. *Am. J. Hum. Genet.* **80,** 186–194 (2007).
8 Arts, H. H., Doherty, D., van Beersum, S. E., Parisi, M. A., Letteboer, S. J., Gorden, N. T. *et al.* Mutations in the gene encoding the basal body protein RPGRIP1L, a nephrocystin-4 interactor, cause Joubert syndrome. *Nat. Genet.* **39,** 882–888 (2007).
9 Cantagrel, V., Silhavy, J. L., Bielas, S. L., Swistun, D., Marsh, S. E., Bertrand, J. Y. *et al.* Mutations in the cilia gene ARL13B lead to the classical form of Joubert syndrome. *Am. J. Hum. Genet.* **83,** 170–179 (2008).
10 Gorden, N. T., Arts, H. H., Parisi, M. A., Coene, K. L., Letteboer, S. J., van Beersum, S. E. *et al.* CC2D2A is mutated in Joubert syndrome and interacts with the ciliopathy-associated basal body protein CEP290. *Am. J. Hum. Genet.* **83,** 559–571 (2008).
11 Coene, K. L., Roepman, R., Doherty, D., Afroze, B., Kroes, H. Y., Letteboer, S. J. *et al.* OFD1 is mutated in X-linked Joubert syndrome and interacts with LCA5-encoded lebercilin. *Am. J. Hum. Genet.* **85,** 465–481 (2009).
12 Davis, E. E., Zhang, Q., Liu, Q., Diplas, B. H., Davey, L. M., Hartley, J. *et al.* TTC21B contributes both causal and modifying alleles across the ciliopathy spectrum. *Nat. Genet.* **43,** 189–196 (2011).
13 Dafinger, C., Liebau, M. C., Elsayed, S. M., Hellenbroich, Y., Boltshauser, E., Korenke, G. C. *et al.* Mutations in KIF7 link Joubert syndrome with Sonic Hedgehog signaling and microtubule dynamics. *J. Clin. Invest.* **121,** 2662–2667 (2011).
14 Garcia-Gonzalo, F. R., Corbit, K. C., Sirerol-Piquer, M. S., Ramaswami, G., Otto, E. A., Noriega, T. R. *et al.* A transition zone complex regulates mammalian ciliogenesis and ciliary membrane composition. *Nat. Genet.* **43,** 776–784 (2011).
15 Huang, L., Szymanska, K., Jensen, V. L., Janecke, A. R., Innes, A. M., Davis, E. E. *et al.* TMEM237 is mutated in individuals with a Joubert syndrome related disorder and expands the role of the TMEM family at the ciliary transition zone. *Am. J. Hum. Genet.* **89,** 713–730 (2011).
16 Lee, J. E., Silhavy, J. L., Zaki, M. S., Schroth, J., Bielas, S. L., Marsh, S. E. *et al.* CEP41 is mutated in Joubert syndrome and is required for tubulin glutamylation at the cilium. *Nat. Genet.* **44,** 193–199 (2012).
17 Lee, J. H., Silhavy, J. L., Lee, J. E., Al-Gazali, L., Thomas, S., Davis, E. E. *et al.* Evolutionarily assembled cis-regulatory module at a human ciliopathy locus. *Science* **335,** 966–969 (2012).
18 Srour, M., Schwartzentruber, J., Hamdan, F. F., Ospina, L. H., Patry, L., Labuda, D. *et al.* Mutations in C5ORF42 Cause Joubert Syndrome in the French Canadian Population. *Am. J. Hum. Genet.* **90,** 693–700 (2012).
19 Zhang, W., Cui, H. & Wong, L. J. Application of next generation sequencing to molecular diagnosis of inherited diseases. *Top. Curr. Chem.* (e-pub ahead of print 11 May 2012; doi:10.1007/128_2012_325).

Supplementary Information accompanies the paper on Journal of Human Genetics website (http://www.nature.com/jhg)

BRIEF REPORT

Human Mutation

OFFICIAL JOURNAL

HGVS HUMAN GENOME VARIATION SOCIETY

www.hgvs.org

KDM6A Point Mutations Cause Kabuki Syndrome

Noriko Miyake,[1]* Seiji Mizuno,[2] Nobuhiko Okamoto,[3] Hirofumi Ohashi,[4] Masaaki Shiina,[5] Kazuhiro Ogata,[5] Yoshinori Tsurusaki,[1] Mitsuko Nakashima,[1] Hirotomo Saitsu,[1] Norio Niikawa,[6] and Naomichi Matsumoto[1]

[1]Department of Human Genetics, Yokohama City University Graduate School of Medicine, Yokohama, Japan; [2]Department of Pediatrics, Central Hospital, Aichi Human Service Center, Kasugai, Japan; [3]Division of Medical Genetics, Osaka Medical Center and Research Institute for Maternal and Child Health, Izumi, Japan; [4]Division of Medical Genetics, Saitama Children's Medical Center, Iwatsuki, Japan; [5]Department of Biochemistry, Yokohama City University Graduate School of Medicine, Yokohama, Japan; [6]Research Institute of Personalized Health Sciences, Health Science University of Hokkaido, Hokkaido, Japan

Communicated by Garry R. Cutting

Received 7 August 2012; accepted revised manuscript 18 September 2012.
Published online 19 October 2012 in Wiley Online Library (www.wiley.com/humanmutation). DOI: 10.1002/humu.22229

ABSTRACT: Kabuki syndrome (KS) is a rare congenital anomaly syndrome characterized by a unique facial appearance, growth retardation, skeletal abnormalities, and intellectual disability. In 2010, *MLL2* was identified as a causative gene. On the basis of published reports, 55–80% of KS cases can be explained by *MLL2* abnormalities. Recently, de novo deletion of *KDM6A* has been reported in three KS patients, but point mutations of *KDM6A* have never been found. In this study, we investigated *KDM6A* in 32 KS patients without an *MLL2* mutation. We identified two nonsense mutations and one 3-bp deletion of *KDM6A* in three KS cases. This is the first report of *KDM6A* point mutations associated with KS.
Hum Mutat 34:108–110, 2013. © 2012 Wiley Periodicals, Inc.

KEY WORDS: Kabuki syndrome; *KDM6A*; point mutations; chromosome X

Kabuki syndrome (KS; MIM# 147920), first described by Niikawa and Kuroki in 1981, is a rare congenital anomaly syndrome with the characteristic facial features of a long palpebral fissure and eversion of lateral third of the inferior eyelids [Kuroki et al., 1981; Niikawa et al., 1981]. Individuals with KS also show mild to severe intellectual disability, growth retardation, skeletal abnormalities, and a variety of visceral malformations. Although KS is thought to inherit in autosomal dominant fashion, other inheritance patterns have also been considered [Matsumoto and Niikawa, 2003]. In 2010, whole exome sequencing successfully identified loss-of-function mutations in *MLL2* in KS. *MLL2* maps to 12q13.12 and consists of at least 54 coding exons. *MLL2* encodes a histone H3 lysine 4 (H3K4)-specific methyl transferase and plays important roles in the epigenetic control of active chromatin states. On the basis of recent reports of *MLL2* mutations in KS, the mutation detection rate of *MLL2* in KS is 55–80% [Banka et al., 2012]. Among the published mutations, 73.2% (170/232) were truncation type, and pathogenic missense mutations were mainly localized in exon 48 [Banka et al., 2012].

X-linked inheritance has also been implicated in KS. Sex chromosome abnormalities in KS have been reported many times and some of the clinical manifestations are shared with Turner syndrome; patients showing overlapping features, called "Turner–Kabuki" syndrome, have been reported [Bianca et al., 2009; Dennis et al., 1993; Niikawa et al., 1988; Rodriguez et al., 2008; Stankiewicz et al., 2001; Wellesley and Slaney, 1994]. Common structural abnormalities (inversion, translocation, and ring chromosome) involving Xp11 and Yp11 in the pseudoautosomal region were observed in KS, implying the potential involvement of the regions for pathogenesis in KS [Matsumoto and Niikawa, 2003]. In addition, two unrelated KS patients with ring X (p11.2q13) have been reported [McGinniss et al., 1997; Niikawa et al., 1988]. However, an X-linked gene for KS has not been identified until recently. In 2012, complete or partial de novo deletions of *KDM6A* (MIM# 300228) were identified in three patients with KS [Lederer et al., 2012]. *KDM6A* resides at Xp11.3 and encodes the lysine demethylase 6A (KDM6A) demethylating di- and trimethyl-lysine 27 on histone H3 (H3K27) [Lee et al., 2007]. H3K4 methylation by MLL2/3 is linked to the demethylation of H3K27 by KDM6A [Lee et al., 2007]. These authors sequenced *KDM6A* in their series of 22 patients, but found no point mutations [Lederer et al., 2012]. In this study, we investigated *KDM6A* with regard to point mutations in KS after obtaining written informed consents from families of patients. The institutional review board of Yokohama City University School of Medicine approved this study.

To identify *KDM6A* mutations in KS, we examined this gene's 29 coding exons along with its exon–intron boundaries (NM_021140.2) in 32 KS individuals with no *MLL2* mutation, using high-resolution melting analysis combined with direct sequencing. We identified three mutations: c.3717G>A (p.Trp1239*) in patient 1 (male, hemizygous), c.1555C>T (p.Arg519*) in patient 2 (male, hemizygous), and c.3354_3356delTCT (p.Leu1119del) in patient 3 (female, heterozygous) (Fig. 1). Nucleotide numbering reflects cDNA numbering with +1 corresponding to the A of the ATG translation initiation codon in the reference sequence (NM_021140.2), according to journal guidelines (www.hgvs.org/mutnomen). The initiation codon is codon 1. One mutation (c.3354_3356delTCT) occurred de novo; parental samples were unavailable for the other two. Because the two nonsense mutations were outside of the last

Additional Supporting Information may be found in the online version of this article.

*Correspondence to: Noriko Miyake, Department of Human Genetics, Yokohama City University Graduate School of Medicine, 3–9 Fukuura, Kanazawa-ku, Yokohama 236–0004, Japan. E-mail: nmiyake@yokohama-cu.ac.jp or Naomichi Matsumoto, E-mail: naomat@yokohama-cu.ac.jp

Contract grant sponsors: Ministry of Health, Labour, and Welfare (Japan) (to N.Mi., H.S., and N.Ma.); Japan Science and Technology Agency (to N.Ma.); Strategic Research Program for Brain Sciences from the Ministry of Education, Culture, Sports, Science, and Technology of Japan (to N.Ma.); Japan Society for the Promotion of Science (to N.Mi., H.S., and N.Ma.); Strategic Research Promotion of Yokohama City University (to N.Ma.); Takeda Science Foundation (to N.Mi. and N.Ma.).

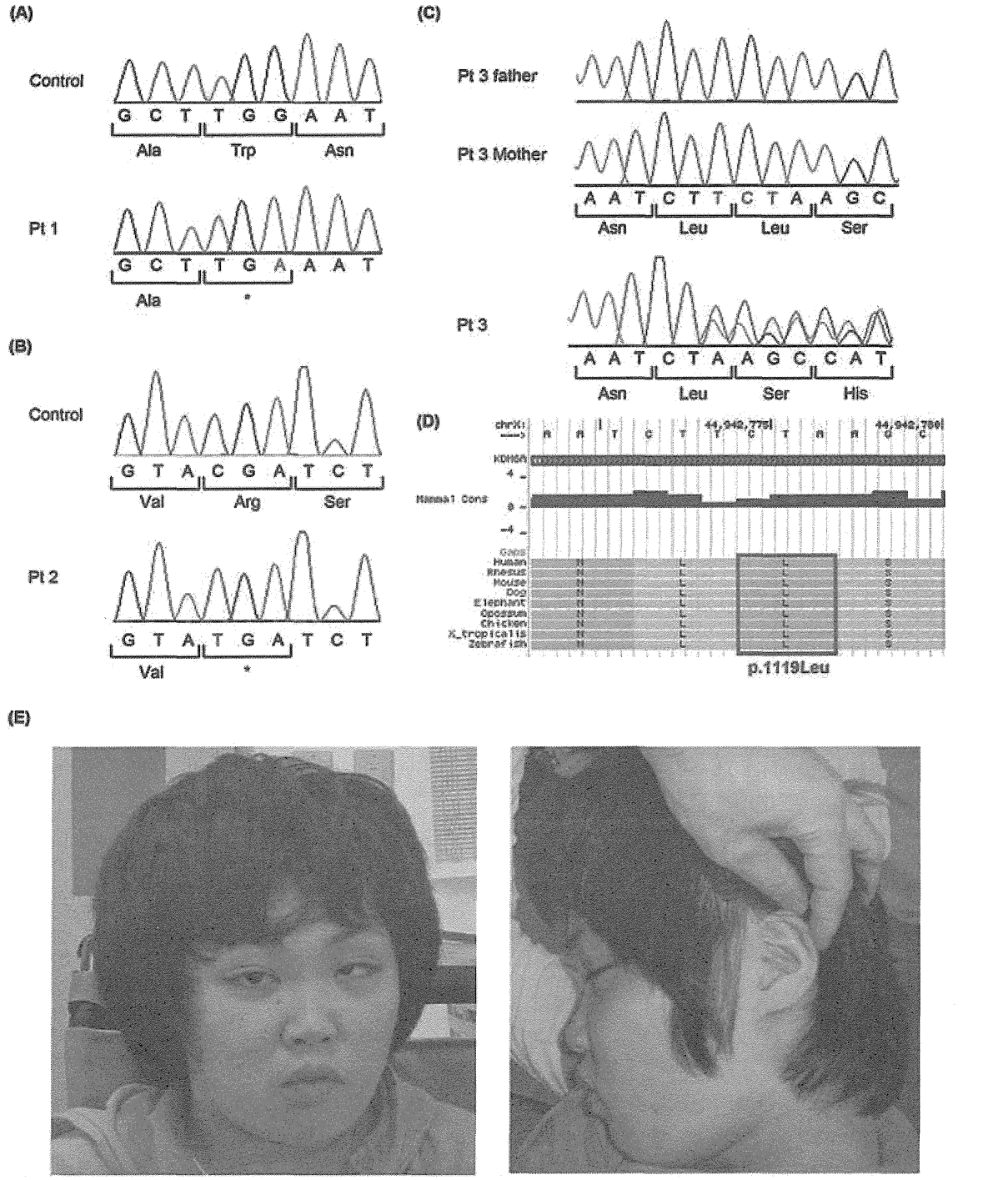

Figure 1. *KDM6A* mutations in three Kabuki syndrome patients. **A–C:** Electropherogram of patient 1: c.3717G>A (p.Trp1239*) (**A**), patient 2: c.1555C>T (p.Arg519*) (**B**), and patient 3: c.3354_3356delTCT (p.Leu1119del) (**C**). Hemizygous changes (**A** and **B**) and a heterozygous change (**C**) can be seen. The altered or deleted nucleotides are written in red. **D:** p. Leu1119 is evolutionarily conserved from zebrafish to human. The position of p.Leu1119 is boxed in red. **E:** Facial photographs of patient 3.

coding exon, and in an exon 55 bp from the 3′ most exon–exon junction, the mutant alleles could be subjected to nonsense-mediated mRNA decay (unfortunately living cells from the patients were unavailable, so we could not test this hypothesis). c.3354_3356delTCT in patient 3 would lead to deletion of one amino acid within the functionally important catalytic Jumonji C (JmjC) domain [Lee et al., 2007]. The amino residue p.Leu1119 is evolutionarily conserved from zebrafish to human (Fig. 1D) and plays an important role in hydrophobic core formation with p.Ile1126 and p.Met1129 to stabilize the JmjC domain [Sengoku and Yokoyama, 2011]. This amino acid deletion may impair helix formation around the mutated residue, resulting in domain destabilization.

Basically, *KDM6A*/*Kdm6a* escapes X-inactivation in humans and mice [Greenfield et al., 1998; Xu et al., 2008]. However, its expression from the inactive X chromosome is lower (15–35%) than that from the active X chromosome in female mice; thus, *Kdm6a* expression

Table 1. Clinical Features of Patients with a *KDM6A* Mutation

	Patient 1	Patient 2	Patient 3
Sex	Male	Male	Female
Mutation	c.3717G>A	c.1555C>T	c.3354_3356delTCT
Protein change	p.Trp1239*	p.Arg519*	p.Leu1119del
De novo status	NA	NA	De novo
Paternal age at birth	34	42	27
Maternal age at birth	33	40	26
Characteristic face	+	+	+
Microcephaly	+	+	–
Long palpebral fissures	+	+	+
Epicanthus	+	–	–
Lower palpebral eversion	+	+	+
Prominent ear	+	+	–
Auricular deformity	+	+	–
Depressed nasal tip	+	+	NA
Short nasal septum	+	+	NA
Abnormal dentition	+	+	–
Hypodontia	+	+	–
High-arched palate	+	+	–
Micrognathia	+	–	–
Short fifth finger	+	–	+
Developmental delay	+ (Severe)	+ (Severe)	+ (Severe)
Intellectual disability	+ (Severe)	+ (Severe)	+ (Severe)
Short stature	+	+	+
Prenatal growth retardation	+ (–1.96 SD)	+	–
Postnatal growth retardation	+	+	+
Cardiovascular abnormality	+	–	–
Joint laxity	+	+	–
Recurrent otitis media	+	–	–
Deafness	+[a]	–	NA
Karyotype	46,XY	46,XY	46,XX

[a]The deafness in patient 1 is conductive because of recurrent otitis media.
KDM6A gene variants were deposited in a gene-specific database (http://www.lovd.Nl/KDM6A).
NA, not analyzed.

in female mice was not twice that in male mice [Xu et al., 2008]. In addition, *UTY* (Yq11.221), a paralog of *KDM6*, has been suspected to partially compensate in males while its function is not well known [Lederer et al., 2012; Xu et al., 2008]. Patient 3 in our study showed a random pattern of X-inactivation with the ratio 57:43 in genomic DNA of peripheral leukocytes. Interestingly, marked skewing of X-inactivation was observed in two female patients reported by Lederer et al. (2012). In their lymphoblast, *KDM6A* deletion was recognized at inactive X chromosome in all 70 mitoses. Here, we propose the threshold model for the pathogenicity of *KDM6A* abnormality (Supp. Fig. S1). The two female patients with a *KDM6A* deletion might not attain the appropriate level of *KDM6A* expression allowing normal development due to existence of specific cells with unfavorable inactivation, whereas male and pure Turner syndrome female with appropriate *KDM6A* expression do not show KS phenotype under assumption of unknown partial functional compensation of *KDM6A* by *UTY* in Y chromosome (only for male) (Supp. Fig. S1).

We reviewed the clinical details of the three patients (Table 1; Supp. Text). All patients were born to unrelated healthy parents. All the three showed severe developmental delay and intellectual disability. Interestingly, patient 3 (female) presented less dysmorphic features and the two male patients 1 and 2 showed a much more severe phenotype with multiple organ involvement (Table 1; Fig. 1E). Null expression of *KDM6A* in males and residual *KDM6A* expression from active X chromosome may explain sex-biased severity (Supp. Fig. S1). Alternatively, it could be explained by a lesser effect of the in-frame mutation in female patient. However, in a previous study, the severity of clinical symptoms varied also among two female patients and a male with a *KDM6A* deletion [Lederer et al., 2012]. More studies of KS patients with *KDM6A* abnormality are necessary. It is likely that the mutation type as well as the X-inactivation pattern in affected organs in females may determine the severity of KS.

In conclusion, we have described the first three point mutations of *KDM6A* in KS. Our three patients out of 32 *MLL2*-negative patients (mutation detection rate: 9.3%) are comparable to the three patients out of 22 *MLL2*-negative patients (13.6%) previously described [Lederer et al., 2012], regardless of the mutation type. The mutation detection rates for *MLL2* (55–80%) plus *KDM6A* (9–13%) in KS suggest that other gene(s) may be found. Because both MLL2 and KDM6A are histone modifiers, the other pathogenic genes might have related functions. Further research is needed to understand the pathomechanisms of KS as well as the role of histone modification in human disease.

Acknowledgments

We thank the patients and their families for participating in this work. We also thank Ms. Y. Yamashita and Ms. S. Sugimoto for technical assistance.

References

Banka S, Veeramachaneni R, Reardon W, Howard E, Bunstone S, Ragge N, Parker MJ, Crow YJ, Kerr B, Kingston H, Metcalfe K, Chandler K, et al. 2012. How genetically heterogeneous is Kabuki syndrome? MLL2 testing in 116 patients, review and analyses of mutation and phenotypic spectrum. Eur J Hum Genet 20:381–388.

Bianca S, Barrano B, Cataliotti A, Indaco L, Ingegnosi C, Ettore G. 2009. Kabuki syndrome and sex chromosomal anomalies: is it really an association? Fertil Steril 91:e6.

Dennis NR, Collins AL, Crolla JA, Cockwell AE, Fisher AM, Jacobs PA. 1993. Three patients with ring (X) chromosomes and a severe phenotype. J Med Genet 30:482–486.

Greenfield A, Carrel L, Pennisi D, Philippe C, Quaderi N, Siggers P, Steiner K, Tam PP, Monaco AP, Willard HF, Koopman P. 1998. The UTX gene escapes X inactivation in mice and humans. Hum Mol Genet 7:737–742.

Kuroki Y, Suzuki Y, Chyo H, Hata A, Matsui I. 1981. A new malformation syndrome of long palpebral fissures, large ears, depressed nasal tip, and skeletal anomalies associated with postnatal dwarfism and mental retardation. J Pediatr 99:570–573.

Lederer D, Grisart B, Digilio MC, Benoit V, Crespin M, Ghariani SC, Maystadt I, Dallapiccola B, Verellen-Dumoulin C. 2012. Deletion of KDM6A, a histone demethylase interacting with MLL2, in three patients with Kabuki syndrome. Am J Hum Genet 90:119–124.

Lee MG, Villa R, Trojer P, Norman J, Yan KP, Reinberg D, Di Croce L, Shiekhattar R. 2007. Demethylation of H3K27 regulates polycomb recruitment and H2A ubiquitination. Science 318:447–450.

Matsumoto N, Niikawa N. 2003. Kabuki make-up syndrome: a review. Am J Med Genet 117C:57–65.

McGinniss MJ, Brown DH, Burke LW, Mascarello JT, Jones MC. 1997. Ring chromosome X in a child with manifestations of Kabuki syndrome. Am J Med Genet 70:37–42.

Niikawa N, Kuroki Y, Kajii T, Matsuura N, Ishikiriyama S, Tonoki H, Ishikawa N, Yamada Y, Fujita M, Umemoto H, Iwama Y, Kondoh I, et al. 1988. Kabuki make-up (Niikawa–Kuroki) syndrome: a study of 62 patients. Am J Med Genet 31:565–589.

Niikawa N, Matsuura N, Fukushima Y, Ohsawa T, Kajii T. 1981. Kabuki make-up syndrome: a syndrome of mental retardation, unusual facies, large and protruding ears, and postnatal growth deficiency. J Pediatr 99:565–569.

Rodriguez L, Diego-Alvarez D, Lorda-Sanchez I, Gallardo FL, Martinez-Fernandez ML, Arroyo-Munoz ME, Martinez-Frias ML. 2008. A small and active ring X chromosome in a female with features of Kabuki syndrome. Am J Med Genet 146A:2816–21.

Sengoku T, Yokoyama S. 2011. Structural basis for histone H3 Lys 27 demethylation by UTX/KDM6A. Genes Dev 25:2266–2277.

Stankiewicz P, Thiele H, Giannakudis I, Schlicker M, Baldermann C, Kruger A, Dorr S, Starke H, Hansmann I. 2001. Kabuki syndrome-like features associated with a small ring chromosome X and XIST gene expression. Am J Med Genet 102:286–292.

Wellesley DG, Slaney S. 1994. Kabuki make-up and Turner syndromes in the same patient. Clin Dysmorphol 3:297–300.

Xu J, Deng X, Watkins R, Disteche CM. 2008. Sex-specific differences in expression of histone demethylases Utx and Uty in mouse brain and neurons. J Neurosci 28:4521–4527.

RESEARCH ARTICLE

Human Mutation

OFFICIAL JOURNAL
HGVS
HUMAN GENOME VARIATION SOCIETY
www.hgvs.org

Mitochondrial Complex III Deficiency Caused by a Homozygous *UQCRC2* Mutation Presenting with Neonatal-Onset Recurrent Metabolic Decompensation

Noriko Miyake,[1]*† Shoji Yano,[2]† Chika Sakai,[3] Hideyuki Hatakeyama,[3] Yuichi Matsushima,[3] Masaaki Shiina,[4] Yoriko Watanabe,[5] James Bartley,[6] Jose E. Abdenur,[7] Raymond Y. Wang,[7] Richard Chang,[7] Yoshinori Tsurusaki,[1] Hiroshi Doi,[1] Mitsuko Nakashima,[1] Hirotomo Saitsu,[1] Kazuhiro Ogata,[4] Yu-ichi Goto,[3] and Naomichi Matsumoto[1]*

[1]*Department of Human Genetics, Yokohama City University Graduate School of Medicine, Yokohama, Japan;* [2]*Genetics Division, Department of Pediatrics, LAC + USC Medical Center, Keck School of Medicine, University of Southern California, Los Angeles, California;* [3]*Department of Mental Retardation and Birth Defect Research, National Institute of Neuroscience, NCNP, Kodaira, Tokyo, Japan;* [4]*Department of Biochemistry, Yokohama City University Graduate School of Medicine, Yokohama, Japan;* [5]*Department of Pediatrics and Child Health, Kurume University School of Medicine, Kurume, Japan;* [6]*Division of Medical Genetics, Department of Pediatrics, Children's Hospital Los Angeles, Los Angeles, California;* [7]*Division of Metabolic Disorders, CHOC Children's, Orange, California*

Communicated by Daniel Nebert

Received 26 June 2012; accepted revised manuscript 7 November 2012.
Published online 19 December 2012 in Wiley Online Library (www.wiley.com/humanmutation). DOI: 10.1002/humu.22257

ABSTRACT: Mitochondrial complex III (CIII) deficiency is a relatively rare disease with high clinical and genetic heterogeneity. CIII comprises 11 subunits encoded by one mitochondrial and 10 nuclear genes. Abnormalities of the nuclear genes such as *BCS1L* and *TTC19* encoding mitochondrial assembly factors are well known, but an explanation of the majority of CIII deficiency remains elusive. Here, we report three patients from a consanguineous Mexican family presenting with neonatal onset of hypoglycemia, lactic acidosis, ketosis, and hyperammonemia. We found a homozygous missense mutation in *UQCRC2* that encodes mitochondrial ubiquinol–cytochrome *c* reductase core protein II by whole-exome sequencing combined with linkage analysis. On the basis of structural modeling, the mutation (p.Arg183Trp) was predicted to destabilize the hydrophobic core at the subunit interface of the core protein II homodimer. In vitro studies using fibroblasts from the index patient clearly indicated CIII deficiency, as well as impaired assembly of the supercomplex formed from complexes I, III, and IV. This is the first described human disease caused by a core protein abnormality in mitochondrial CIII.
Hum Mutat 34:446–452, 2013. © 2012 Wiley Periodicals, Inc.

KEY WORDS: mitochondrial complex III (CIII); *UQCRC2*; whole exome sequence; supercomplex

Introduction

The mitochondrial respiratory chain generates energy as ATP by means of the electron-transport chain and the oxidative-phosphorylation system. The mitochondrial respiratory chain, located in the inner mitochondrial membrane, is composed of five multimeric protein complexes: I, II, III, IV, and V. Among them, the complex III (CIII) (bc1 complex or ubiquinol–cytochrome *c* reductase; EC1.10.2.2) monomer is composed of 11 proteins [Iwata et al., 1998]. One protein is encoded by mitochondrial DNA (*MTCYB*) and the other 10 are encoded by nuclear DNA. The latter are categorized into three groups: (1) core proteins (encoded by *UQCRC1* and *UQCRC2*), (2) respiratory proteins (*CYC1* and *UQCRFS1*), and (3) low-molecular-weight proteins (*UQCRH*, *UQCRB*, *UQCRQ*, *UCRC*, *UQCR11*, and *UQCRFS1*). In its native state, the CIII monomer is quickly converted into a catalytically active homodimer that is incorporated into a supercomplex (respirasome) with complexes I and IV, and this supercomplex functions as a single enzyme [Schagger and Pfeiffer, 2000].

Mitochondrial CIII enzyme deficiency (CIII deficiency; MIM# 124000) is a relatively rare disease with clinical and genetic heterogeneity. Until now, mutations in four genes have been known to cause autosomal recessive CIII deficiencies: *UQCRB* (NM_006294), *UQCRQ* (NM_014402), *BCS1L* (NM_004328), and *TTC19* (NM_017775). *UQCRB* and *UQCRQ* encode components of CIII itself, whereas *BCS1L* and *TTC19* produce mitochondrial assembly factors. Although recessive *BCS1L* mutations are the most frequent cause of CIII deficiency, the majority of the genetic causes of CIII deficiency remain unknown [Benit et al., 2009; de Lonlay et al.,

Additional Supporting Information may be found in the online version of this article.

†These authors contributed equally to this work.

*Correspondence to: Noriko Miyake, Department of Human Genetics, Yokohama City University Graduate School of Medicine, 3-9 Fukuura, Kanazawa-ku, Yokohama 236-0004, Japan. E-mail: Noriko Miyake: nmiyake@yokohama-cu.ac.jp; or Naomichi Matsumoto, Department of Human Genetics, Yokohama City University Graduate School of Medicine, 3-9 Fukuura, Kanazawa-ku, Yokohama 236-0004, Japan. E-mail: naomat@yokohama-cu.ac.jp

Contract grant sponsors: Ministry of Health, Labor, and Welfare; the Japan Science and Technology Agency; the Strategic Research Program for Brain Sciences; Ministry of Education, Culture, Sports, Science, and Technology of Japan; the Japan Society for the Promotion of Science; 2011 Strategic Research Promotion of Yokohama City University; the Japan Epilepsy Research Foundation; and the Takeda Science Foundation.

2001; DiMauro and Schon, 2003; Fernandez-Vizarra et al., 2007; Hinson et al., 2007; Visapaa et al., 2002]. Interestingly, *BCS1L* mutations cause variable clinical presentations: Bjornstad syndrome (MIM# 262000), which is characterized by sensorineural hearing loss and pili torti [Hinson et al., 2007]; GRACILE syndrome (MIM# 603358), which presents with fetal growth retardation, aminoaciduria, cholestasis, iron overload, lactic acidosis, and early death [Visapaa et al., 2002]; and Leigh syndrome (MIM# 256000) [de Lonlay et al., 2001]. A homozygous mutation of *TTC19* causes a progressive neurodegenerative disorder [Ghezzi et al., 2011]. A homozygous 4-bp deletion of *UQCRB* causes hypoglycemia and lactic acidosis [Haut et al., 2003] and a homozygous missense mutation of *UQCRQ* results in severe psychomotor retardation, extrapyramidal signs, and dementia [Barel et al., 2008].

Here, we describe the first human mutation of *UQCRC2* encoding core protein 2 of CIII, utilizing linkage analysis and whole-exome sequencing.

Materials and Methods

DNA Preparation

DNAs from family members and fibroblasts from patients were collected after obtaining informed consent. DNA was extracted from blood leukocytes using a QIAamp DNA Blood Midi Kit (Qiagen, Hilden, Germany) or QuickGene-610L (Fujifilm, Tokyo, Japan), according to the manufacturers' instructions. DNAs from 80 Mexican control subjects were purchased from the Coriell Institute for Medical Research (Camden, New Jersey). The experimental protocols were approved by the institutional review board of Yokohama City University.

Linkage Analysis

SNP typing was performed using an Affymetrix Human Mapping SNP 10K Xba I 142 2.0 array (Affymetrix, Santa Clara, California), according to the manufacturer's instructions. A multipoint linkage analysis was performed using Allegro version 2.0 [Gudbjartsson et al., 2005]. An autosomal recessive mode of inheritance with complete penetrance and a disease allele frequency of 0.005 was used.

Exome Sequence

Briefly, 3 μg of genomic DNA was sheared and captured using a NimbleGen SeqCap EZ Exome Library SR (Roche NimbleGen, Inc., Madison, New Jersey), according to the manufacturer's instructions. The captured sample was sequenced on a GAIIx instrument (Illumina, Inc., San Diego, California) using 76-bp paired-end reads. Image analysis and base calling were performed by sequence-control software real-time analysis (Illumina, Inc.) and CASAVA software v1.7 (Illumina, Inc.). The quality-controlled (path-filtered) reads were mapped to human genome reference hg19 with Mapping and Assembly with Qualities (MAQ; http://maq.sourceforge.net/) and NextGENe software v2.00 (SoftGenetics, State College, Pennsylvania). The variants from MAQ were annotated by SeattleSeq annotation 131 (http://snp.gs.washington.edu/SeattleSeqAnnotation131). The priority scheme of the variants was described previously [Tsurusaki et al., 2011]. The nucleotide numbering of the variants reflects the cDNA numbering, with +1 corresponding to the A of the ATG translation initiation codon in the reference sequence, according to journal guidelines (www.hgvs.org/mutnomen). The initiation codon is codon 1.

Expression Vector Preparation

For construction of a mammalian expression vector, full-length *UQCRC2* (NM_003366.2) was amplified from a cDNA library from a multiple-tissue cDNA (MTC) panel (Clontech, Mountain View, California) using KOD-plus DNA polymerase (Toyobo, Osaka, Japan). The PCR product was cloned into the entry vector (pDONR^{TM}221) of the gateway system (Invitrogen, Carlsbad, California). Each of the two missense mutations was independently introduced into the entry clone using a QuickChange II XL site-directed mutagenesis kit (Stratagene, La Jolla, California). Each insert was cloned into pcDNA-DEST40 (C-terminal V5 and 6xHis tag) by LR recombination. All the clones were verified by direct sequencing. In addition, full-length *UQCRC2* (wild type, mutant, or SNP [rs4850: c.548G>A, p.Arg183Gln]) and AcGFP constructs were cloned into multiple cloning sites A and B of the pIRES vector (Clontech).

Intracellular Localization

Each mammalian expression construct (200 ng) was transfected into COS-1 cells using FuGENE6 (Roche Diagnostics, Indianapolis, Indiana). After 24 hr of transfection, MitoTracker Red CMXRos (Invitrogen) was added and incubated for 30 min. The cells were then fixed with 4% paraformaldehyde for 20 min at room temperature. After permeabilization with 0.1% Triton/1× PBS for 10 min, C-terminally V5-6xHis-tagged UQCRC2 protein was stained with a mouse anti-V5 antibody (1:1,000) (Invitrogen) and an Alexa Fluor 488-conjugated goat antimouse IgG secondary antibody (1:1,000) (Molecular Probes, Carlsbad, California). Confocal images were taken with a FLUOVIEW FV1000-D microscope (Olympus, Tokyo, Japan).

Mitochondrial Enzyme Activity Assay

Mitochondrial enzyme activities were measured using a previously reported method [Trounce et al., 1996], with slight modifications. The complex I activity is indicated as the rotenone-sensitive NADH–CoQ1 reductase activity. In control assays, the activity was decreased to 20% by rotenone.

Western Blotting

Mitochondrial enzyme activity and supercomplex formation were analyzed by western blotting. The enzyme activities of the mitochondrial respiratory chain complexes were measured using mitochondrial fractions prepared from primary fibroblasts derived from patient 1 ($n = 3$) and control subjects ($n = 10$). Each measurement was basically performed in triplicate (if the available materials allowed). The values were normalized to complex II or citrate synthase. Immunoblot detection of each respiratory chain complex was performed using mitochondria solubilized with 0.5% *n*-dodecyl-β-D-maltoside (DDM). The same amount of pooled mitochondrial protein from control subjects ($n = 10$) was used as the control. The primary antibodies used were as follows: 2 μg/ml anti-NDUFA9 (complex I; Invitrogen), 0.02 μg/ml anti-SDHA (complex II; Invitrogen), 2 μg/ml anti-UQCRC1 (CIII; Abcam, Cambridge, Massachusetts), 0.2 μg/ml anti-MTCO1 (complex IV; Invitrogen), and

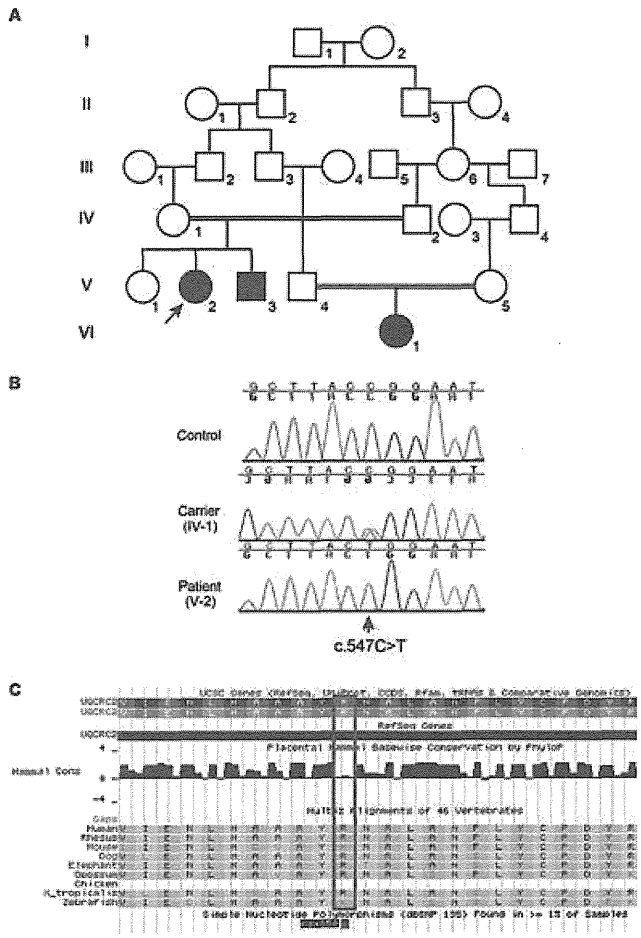

Figure 1. Identification of a *UQCRC2* mutation in a consanguineous Mexican family. **A:** Pedigree of the reported family. The arrow indicates the proband. **B:** Electropherogram of the c.547C>T *UQCRC2* mutation. All three patients (1, 2, and 3) showed a homozygous change, whereas the parents and an unaffected sibling of patients 1 and 2 were heterozygous carriers. The arrow indicates c.547C>T. **C:** Evolutionary conservation of p.Arg183 in UQCRC2 outlined in red. rs4850 (chr 16: 21976762, G>A, p.Arg183Gln) is a common SNP based on the dbSNP135 database.

2 μg/ml anti-ATP5B (complex V; Invitrogen). Immunoblot detection of the respiratory supercomplex was performed using mitochondria solubilized with 1% (w/v) digitonin. The same amount of pooled mitochondrial protein from control subjects (n = 10) was used as the control. The primary antibodies used were as follows: 0.02 μg/ml anti-SDHA (complex II; Invitrogen) and 2 μg/ml anti-UQCRC1 (CIII; Abcam). The band intensity of the supercomplex was estimated by densitometry and normalized to that of complex II. The data were obtained by three independent assays.

Results

Patient 1 (V:2 in Fig. 1A) is a Hispanic female born to a 26-year-old healthy female (G2P2Ab0) and a 28-year-old healthy male who are second cousins. She was delivered at 37 weeks by Cesarean section because of a pathological cardiotocogram. At birth, she weighed 2,329 g (5–10th percentile) with a length of 46 cm (5–10th percentile), and her occipitofrontal circumference was 34 cm (25–50th percentile). Her Apgar scores were 8, 9, and 9 at 1, 5, and 10 min, respectively. She developed a severe metabolic acidosis (pH 7.1, with a base excess of −24.6 mEq/l) within 1 day, requiring admission to a neonatal intensive care unit. Blood lactate and pyruvate on admission were 25.5 mM (reference range: <2.2 mM) and 0.436 mM (reference range: <0.16 mM), respectively (lactate to pyruvate ratio = 58.48). Clinical examination revealed tachypnea (47 breaths/min), tachycardia (181 beats/min), mild subcostal retractions, Levine II/VI systolic cardiac murmur, no organomegaly, and poor sucking reflex. Blood ammonia was 126 μM (reference range in neonates: <80 μM). The patient responded promptly to supportive therapy, with intravenous glucose infusion providing 10 mg/kg/min and a sodium bicarbonate drip improving the blood lactate level down to 12.7 mM within 24 hr. The lactate and pyruvate levels further improved to 3.1 and 0.125 mM within 3 days, respectively. Urine organic acid analysis on admission was remarkable for massive lactic and pyruvic aciduria, as well as ketonuria. Plasma amino acids were remarkable for a high alanine level (1,519 μM; reference range: 200–600 μM). Magnetic resonance imaging (MRI) of the brain revealed small right parietal and temporal infarcts.

She recovered without sequelae and was discharged on full oral feeds with a high-carbohydrate, reduced-fat formula (60% of calories from carbohydrate, 30% of calories from fat) after 1.5 months of hospitalization. She was also diagnosed with an atrial septal defect and renal tubular acidosis. After the initial hospitalization, she was hospitalized more than 10 times because of episodic metabolic decompensation with lactic acidosis (highest value was 10.8 mM at the age of 3 years and 10 months), hyperammonemia (highest value was 346 μM at the age of 3 years and 3 months), ketosis, and hypoglycemia, which were triggered by intercurrent illnesses including fevers, vomiting, and diarrhea. The patient is now 5 years of age, with normal growth and no signs of intellectual disability. The frequency of hospitalization has decreased, although she still requires urgent medical treatment with intravenous glucose infusion to prevent metabolic decompensation during intercurrent illnesses.

Patient 2 (V:3 in Fig. 1A) is a younger full sibling of patient 1. He was born at 39 weeks of gestation by repeat Cesarean section. At birth, he weighed 2,658 g (5–10th percentile) with a length of 49 cm (25–50th percentile), and his occipitofrontal circumference was 34.3 cm (25th percentile). His Apgar scores were 8 and 9 at 1 and 5 min, respectively. He developed tachypnea, grunting, and poor feeding within 1 day because of lactic acidemia. The initial capillary blood gas showed a pH of 7.05, pCO_2 of 25 mmHg, bicarbonate of 5.8 mmol/l, and a base excess of −22 mEq/l. He was intubated for 2 days and treated with intravenous glucose infusion and a bicarbonate drip to correct the metabolic acidosis. Feeding with a high-carbohydrate, reduced-fat formula was started in 10 days. His initial hospitalization was 1-month long, during which he was diagnosed with congenital lactic acidemia and persistent hypoglycemia of unknown etiology. He was treated with corticosteroid replacement therapy owing to adrenal insufficiency for 4 months until a normal adrenocorticotropic hormone stimulation test was obtained. At the age of 8 months, he was found unresponsive after 6 hr of fasting owing to decreased appetite associated with a 2-day mild upper-respiratory-tract infection. At a local emergency room, metabolic acidosis (pH 7.23), hypoglycemia (3 mg/dl; reference range: >60 mg/dl), and hyperammonemia (463 μM), as well as ketosis (blood and urine), were noted. He had five episodes of generalized seizure associated with this episode. Following treatment with levetiracetam, he has been seizure free. Brain MRI findings at the age of 8 months were unremarkable. He was hospitalized for 1 month and discharged without sequelae, and had more than 10 hospitalizations because of similar episodes of lactic acidosis, hypoglycemia, hyperammonemia, and ketosis triggered by intercurrent illnesses. Developmental delay was noted once at 4 months of age. Following

physical and speech therapy, his development was later evaluated as normal at 3 years of age. He is now 4 years of age, with normal growth and no signs of intellectual disability. Physical examination revealed neither dysmorphic features nor abnormal focal neurological signs. He has been fed with a reduced-fat, high-carbohydrate diet and fasting precautions. The frequency of hospitalization has decreased, although he continues to require urgent medical treatment with intravenous glucose infusion to prevent metabolic decompensation during intercurrent illnesses. Laboratory study data obtained in the acute severe metabolic decompensation stage at 16 months of age were remarkable, which are as follows: pH 7.19 capillary blood gas, 11 mg/dl glucose, 348 μM blood ammonia, and 6.8 mM blood lactate. Urine organic acid analysis showed markedly elevated 3-hydroxybutyrate and acetoacetate indicating severe ketosis, markedly elevated lactate and pyruvate indicating lactic acidosis, markedly elevated dicarboxylic acids (adipic acid, 1,194 mmol/mol Cr [reference range: <15 mmol/mol Cr], suberic acid, 122 mmol/mol Cr [reference range: <7 mmol/mol Cr], sebacic acid, 288 mmol/mol Cr [reference range: <2 mmol/mol Cr]) indicating hyperactive fatty acid beta oxidation, and moderately elevated tricarboxylic acid cycle intermediates including malate, fumarate, and 2-oxoglutarate. Plasma amino acids showed elevated alanine at 440 μM (reference range: 23–410 μM). Acylcarnitine profiles obtained at 19 months of age in mild decompensation showed marked elevation of C2 (48 nmol/ml [reference range: 2.6–15.5 nmol/ml]) and moderate elevation of 3-hydroxyacylcarnitines (C12–C18).

Patient 3 (VI:1 in Fig. 1A) is a girl born to consanguineous parents within the same pedigree as patients 1 and 2, but in a different branch. She was small for gestational age and was born vaginally to a 23-year-old mother after a full-term gestation. Her birth weight was 2,200 g. Initially, she had mild respiratory distress and required 1 additional day of monitoring. By 18 months of age, she had undergone four hospitalizations for vomiting, dehydration, and hypoglycemia. An initial blood examination at 18 months of age showed that her blood glucose was 17 mg/dl, bicarbonate was 8 mmol/l, and anion gap was 30 mmol/l. The simultaneous blood lactate and pyruvate levels were 26.3 mg/dl (reference range: <16.0 mg/dl) and 1.5 mg/dl (reference range: <1.5 mg/dl), respectively. She responded quickly to intravenous dextrose with correction of the hypoglycemia and metabolic acidosis. She had developmental delay and microcephaly (second percentile) that led to a brain MRI, but this was interpreted as normal. At 18 months, she spoke only two words but could follow two-part commands. She walked at 15 months of age and had low body weight until starting occupational therapy at 14 months of age. She was not dysmorphic. Her muscle strength and tone were normal when she was in good health, allowing her to climb, hop, and jump in a manner appropriate for her age.

Considering the consanguinity in this family, we hypothesized that the disease was inherited in an autosomal recessive fashion. Linkage analysis using two patients (1 and 2) and three unaffected family members (IV:1, IV:2, and V:1) indicated that homozygous regions totaling 36-Mb were shared by the two affected individuals with logarithm of the odds scores ≥2.0, as calculated by Allegro version 2 [Gudbjartsson et al., 2005] (Supp. Table S1). We then performed whole-exome sequencing of DNA from patient 1. Two homozygous variants within the 36-Mb homozygous regions were identified: c.547C>T, p.Arg183Trp in *UQCRC2* (NM_003366) and c.1675A>G, p.Met559Val in *TNRC6A* (NM_014494). Sanger sequencing confirmed the two variants in patient 1. The Polyphen-2 program (http://genetics.bwh.harvard.edu/pph2/) predicted that p.Arg183Trp in *UQCRC2* and p.Met559Val in *TNRC6A* were probably damaging and benign, respectively (Table 1). *TNRC6A* was ruled out as a candidate because the heterozygous *TNRC6A* change was found in patient 3. *UQCRC2* encodes ubiquinol–cytochrome *c* reductase core protein II (UQCRC2; MIM# 191329), a core protein of CIII. All three patients possessed the homozygous p.Arg183Trp change in *UQCRC2*, whereas the father (IV-2), mother (IV-1), and sister (V-1) (all unaffected) were heterozygous (Fig. 1B). This change was not observed among 80 Mexican control alleles or 750 Japanese control alleles.

Table 1. Prediction of Mutational Effects in UQCRC2

Mutation	Alteration	Type	Grantham score[a]	Polyphen-2	Energy ddG[b]
c.547C>T	p.Arg183Trp	Mutant	101	0.998	10.02
c.548G>A	p.Arg183Gln	SNP	43	0.177	2.19
c.547_548CG>AA	p.Arg183Lys	Ortholog	26	0.001	1.74

[a]Grantham score indicates the chemical dissimilarity caused by codon replacements.
[b]The corrected average interaction energy ddG of each altered amino acid is calculated by FoldX as homozygous mutation.

To predict the effect of the missense mutation (c.547C>T, p.Arg183Trp) on the structural stability of CIII, we calculated the free-energy change of interactions between the core protein monomers (encoded by *UQCRC2*) with and without the mutation using FoldX software (version 3.0) [Guerois et al., 2002; Khan and Vihinen, 2010]. For this calculation, we used the crystal structure of bovine CIII (PDB code 2A06) as a structural model because no crystal structure is available for human UQCRC2. Amino acid position 183 of UQCRC2 is a highly conserved basic amino acid among species from zebrafish to humans (e.g., Arg in humans and cows, Lys in mice; Fig. 1C) and is reported to be substituted for Gln as a nonsynonymous human SNP (rs4850 [c.548G>A, p.Arg183Gln]) (Fig. 1C). Therefore, we also calculated the interaction-energy change upon replacement of Arg183 with Lys or Gln, in addition to the Trp found in the patient. The calculated interaction-energy change caused by replacement of Arg183 with Trp was estimated as 10 kcal/mol, whereas those caused by replacement with Lys or Gln were no more than 2 kcal/mol (Fig. 2A, Table 1). The molecular structure of the wild-type core protein homodimer indicated that the methylene part of the Arg183 side chain of one subunit forms a hydrophobic core with the side chains of His254 and Phe449 of the other subunit at the homodimer interface (Fig. 2B and C). When the Arg183 of the core protein was replaced by Trp, the introduced Trp183 side chain flipped outward from the original side-chain position because of steric hindrance (Fig. 2D). In contrast, when Arg183 was replaced by Lys or Gln, each side chain occupied the original position to maintain a hydrophobic core with the methylene part of Lys or Gln (Fig. 2E and F). This indicates that the Arg183Trp mutation in UQCRC2 would disrupt the hydrophobic core formed at the interface of the UQCRC2-containing complex, resulting in destabilization of CIII. In vitro experiments showing that the exogenous and endogenous expressions of the UQCRC2 mutant were significantly reduced (Supp. Figs. S1 and S2) may support the protein instability.

To test whether this mutation alters UQCRC2 localization at the mitochondrial inner membrane, we created mammalian full-length wild-type, mutant, and SNP (rs4850) constructs; transiently overexpressed them in COS1 cells; and observed their localization microscopically. The mutant protein colocalized with mitochondria, similar to the wild-type and SNP proteins (Supp. Fig. S3). This indicates that the p.Arg183Trp mutation probably does not alter the intracellular localization.

To evaluate mitochondrial function in vitro, we measured the enzyme activities of the mitochondrial respiratory chain complexes

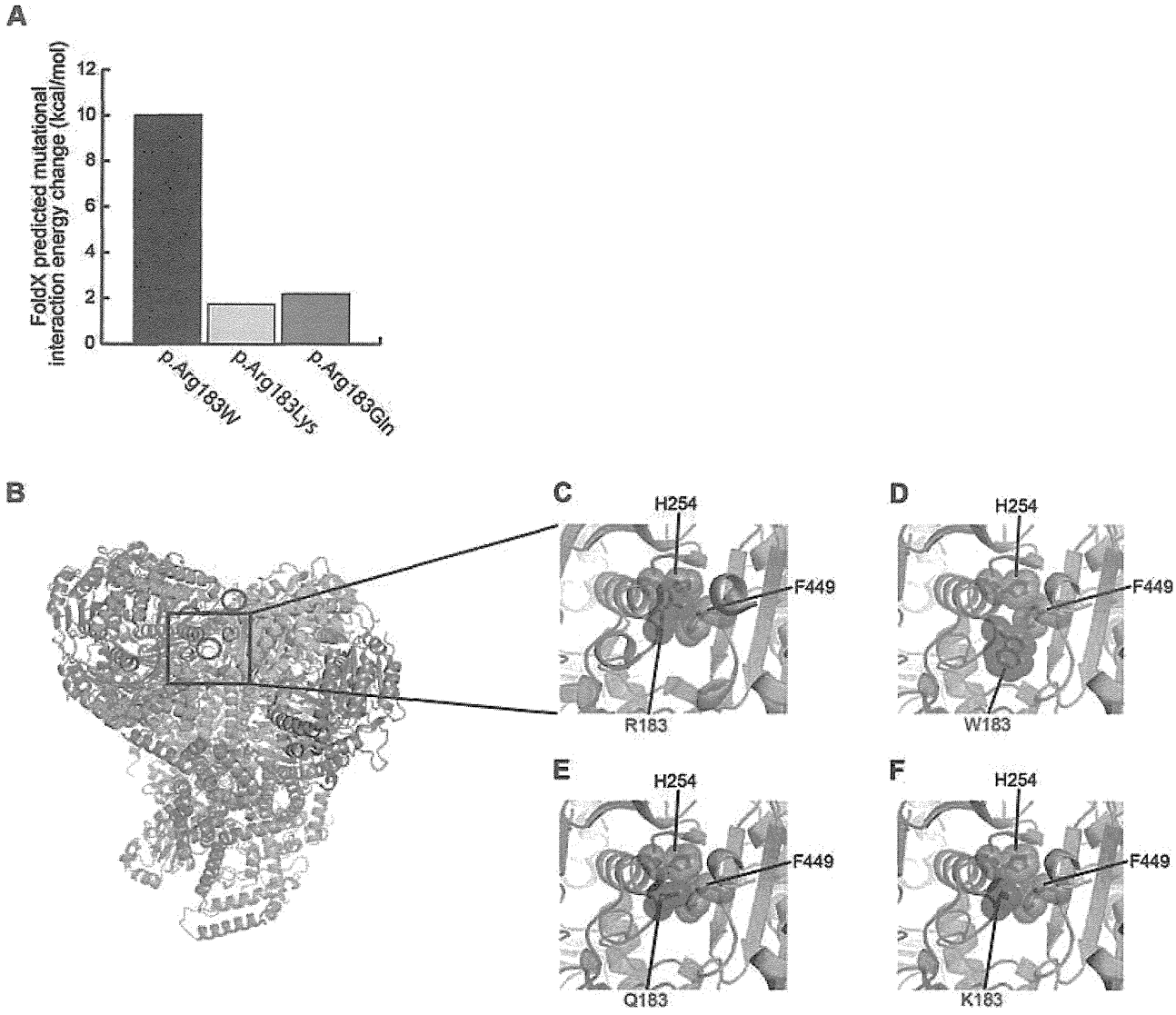

Figure 2. Molecular structural consideration of the effect on dimerization of amino acid replacement at residue position 183 in the core protein. **A:** Calculated interaction-energy change of the core protein homodimer upon replacement by the indicated amino acids at residue 183 using FoldX software. **B:** Overview of the crystal structure of the bovine mitochondrial bc1 (CIII) complex (PDB code 2A06). The core protein monomers are colored green and cyan; the other components are shown in gray. The helices, strands, and loops are shown as ribbons, arrows, and threads, respectively. The red circle indicates residue 183 in the core protein. The box corresponds to the enlarged areas shown in parts (**C**)–(**F**). **C–F:** Detailed views of the core protein homodimerization interface in the wild-type (**C**) and mutated, polymorphic, orthologous (p.Arg183Trp/Gln/Lys) (**D, E, F,** respectively) complex structures. The residues at amino acid 183 of one subunit (red), and His254 and Phe449 of the other subunit (orange) are shown as sticks with Connolly surfaces. All graphics were drawn using PyMOL (www.pymol.com).

using mitochondrial fractions prepared from primary fibroblasts derived from patient 1. With normalization to complex II activity, the CIII activity of patient 1 was decreased to 50% of that in the control subjects (n = 10), whereas complex I activity increased by threefold and complex IV activity remained at the same level as in the control subjects (Fig. 3A). Similar results were obtained using normalization to citrate synthase activity (Fig. 3B). We also investigated the steady-state level of the respiratory complexes by blue-native polyacrylamide gel electrophoresis (BN-PAGE) using the same mitochondrial fraction used for the enzyme activity measurements. For analysis of individual complexes, mitochondria were solubilized with 0.5% (w/v) DDM. For analysis of the supercomplex (complexes I, III, and IV), mitochondria were solubilized with 1% (w/v) digitonin. After BN-PAGE, we performed immunoblotting with specific antibodies for the respiratory complexes (Fig. 3C–F, Supp. Notes, and Supp. Fig. S4). In the patient's fibroblasts, we found that CIII and supercomplex assembly were decreased to 18%–20% $\gg$ 22% –23% (Fig. 3C and D) and 4% $\gg$ 7.5% (Fig. 3E and F) of the levels in pooled control samples, respectively. These data indicate that a homozygous missense mutation (c.547C>T, p.Arg183Trp) in *UQCRC2* causes moderately impaired CIII function and severely decreased amounts of CIII and supercomplex, which would be the primary molecular pathogenesis in the patients.

Discussion

Among the genes known to cause CIII deficiency, impairment of UQCRC2, as found in our patients, leads to a similar clinical course to that reported for UQCRB defects with recurrent crises of

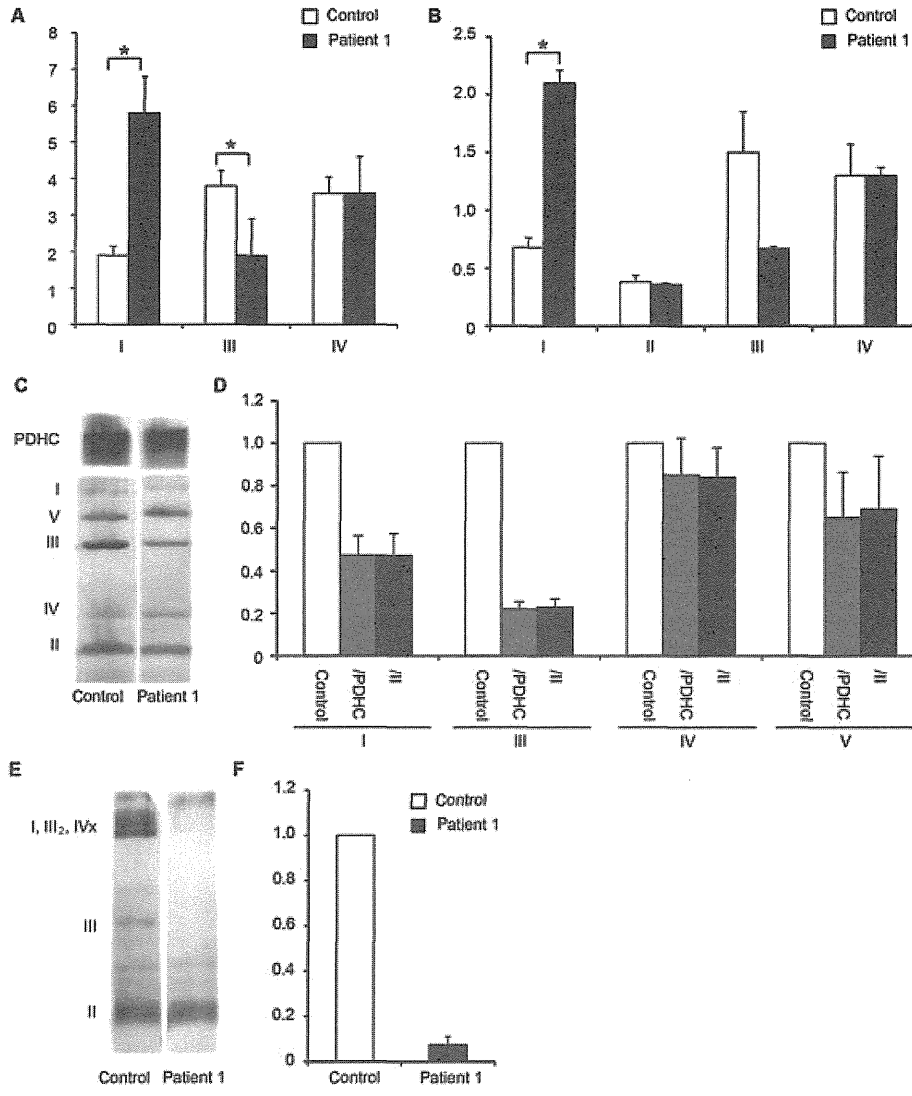

Figure 3. Mitochondrial enzyme activity and supercomplex formation. **A, B:** Enzyme activities of the mitochondrial respiratory chain complexes using mitochondrial fractions prepared from primary fibroblasts derived from patient 1 ($n = 3$) and control subjects ($n = 10$). Each measurement was performed in triplicate. The values were normalized to complex II (**A**) or citrate synthase (**B**). Error bars represent the SEM. **C, D:** Immunoblot detection of each respiratory chain complex using mitochondria solubilized with 0.5% DDM. The same amount of pooled mitochondrial protein from control subjects ($n = 10$) was loaded into the control lane. The band intensity of each respiratory complex was estimated by densitometry and normalized to that of PDHC (gray bar) or complex II (black bar). The data were obtained by three independent assays and the error bars in (**D**) represent the SEM. **E, F:** Immunoblot detection of the respiratory supercomplex using mitochondria solubilized with 1% (w/v) digitonin. The same amount of pooled mitochondrial protein from control subjects ($n = 10$) was loaded into the control lane. The band intensity of the supercomplex was estimated by densitometry and normalized to that of complex II (black bar). The data were obtained by three independent assays and the error bars in (**F**) represent the SEM.

hypoglycemia, lactic acidosis, and ketosis, although the latter did not show hyperammonemia. In contrast, impairment of BCS1L, TTC19, and UQCRQ leads to rather severe complications such as intrauterine growth retardation, liver failure, tubulopathy, sensorineural hearing loss, and abnormalities on brain MRI. The normal development in our patients, despite frequent metabolic crises, may suggest that the UQCRC2 phenotype in our family is milder than disorders of the CIII genes and that this UQCRC2 abnormality does not primarily affect the brain. However, patients 2 and 3 showed epilepsy, and developmental delay was noted in patient 3. It remains to be seen whether this clinical variability is caused by variable expressivity, unknown modifiers, or secondary to the severity of the acute metabolic crises. Interestingly, our patients showed hyperammonemia, highly abnormal urine organic acids indicative of mitochondrial dysfunction, and highly elevated plasma hydroxyl fatty acids during their crises, whereas patients with the other reported CIII impairment disorders did not [Barel et al., 2008; de Lonlay et al., 2001; Ghezzi et al., 2011; Haut et al., 2003; Hinson et al., 2007; Visapaa et al., 2002]. These observations may imply that *UQCRC2* mutations have secondary effects in other metabolic pathways including the Krebs cycle, beta oxidation, and urea cycle.

Conclusion

We have identified, for the first time, a homozygous mutation in human *UQCRC2* encoding a core protein of mitochondrial CIII. Further studies of additional patients with *UQCRC2* abnormalities are necessary to fully understand human CIII disorders.